

Mechanisms of antibiotic action shape the fitness landscapes of resistance mutations

Colin Hemez^{1,2}, Fabrizio Clarelli^{3,4}, Adam C. Palmer⁵, Leonid Chindelevitch⁶, Theodore Cohen⁷, and Pia Abel zur Wiesch^{3,4,8*}*

¹ Systems Biology Institute, Yale University, West Haven, CT USA 06516

² Department of Molecular, Cellular, and Developmental Biology, Yale University, New Haven, CT USA 06520

³ Institute of Pharmacy, Arctic University of Norway, Tromsø, Norway 9017

⁴ Center for Infectious Disease Dynamics, Department of Biology, Pennsylvania State University, University Park, PA USA 16802

⁵ Department of Pharmacology, Computational Medicine Program, Lineberger Comprehensive Cancer Center, University of North Carolina at Chapel Hill, Chapel Hill, NC USA 27599

⁶ School of Computing Science, Simon Fraser University, Burnaby, BC, Canada V5A 1S6

⁷ Department of Epidemiology of Microbial Diseases, Yale School of Public Health, New Haven, CT USA 06520

⁸ Centre for Molecular Medicine Norway, Nordic EMBL Partnership, Oslo, Norway 0318

* Correspondence to colin.hemez@yale.edu, pia.z.wiesch@uit.no

1 **Abstract**

2 Antibiotic-resistant pathogens are a major public health threat. Understanding how an
3 antibiotic's mechanism of action influences the emergence of resistance could help to
4 improve the design of new drugs and to preserve the effectiveness of existing ones. To this
5 end, we developed a model that links bacterial population dynamics with antibiotic-target
6 binding kinetics. Our approach allows us to derive mechanistic insights on drug activity from
7 population-scale experimental data and to quantify the interplay between drug mechanism
8 and resistance selection. We find that whether a drug acts as a bacteriostatic or bactericidal
9 agent has little influence on resistance selection. We also show that heterogeneous drug-
10 target binding within a population enables antibiotic-resistant bacteria to evolve secondary
11 mutations, even when drug doses remain above the resistant strain's minimum inhibitory
12 concentration. Our work suggests that antibiotic doses beyond this "secondary mutation
13 selection window" could safeguard against the emergence of high-fitness resistant strains
14 during treatment.

15

16 (word count: 150)

17

18

19 Introduction

20 The emergence and spread of antibiotic-resistant bacterial pathogens is an urgent global
21 problem that threatens to undermine one of the most essential components of modern
22 medicine (WHO, 2012). Antibiotic resistance is also expensive, adding an average of US \$1400
23 to the costs of treatment for each of the 2.8 million patients who become infected with a drug-
24 resistant bacterium in the United States annually (CDC, 2019; Thorpe, Joski, & Johnston, 2018;
25 WHO, 2014). The scarcity of promising new antimicrobial drugs with novel mechanisms of
26 action further exacerbates the challenges associated with managing the spread of drug
27 resistance (Roberts, Kruger, Paterson, & Lipman, 2008; Silver, 2011). Given the increasing
28 incidence of resistant bacterial infections and the lack of new drugs on the horizon, clinicians,
29 researchers, and global leaders must act to preserve the effectiveness of the world's existing
30 antibiotic drug arsenal (WHO, 2012).

31 Antibiotic treatment induces a strong selective pressure on bacterial populations to
32 evolve resistance (Hughes, 2014; Rao, 1998). Resistance mutations raise the minimum
33 inhibitory concentration (MIC) of an antibiotic, the amount of drug needed to suppress the
34 growth of a bacterial culture (Andrews, 2001). However, alleles that confer drug resistance also
35 frequently carry fitness costs (Andersson & Hughes, 2010; Melnyk, Wong, & Kassen, 2015;
36 Vogwill & MacLean, 2015), predominantly because antibiotics target vital cellular functions
37 (such as DNA replication and protein synthesis). Resistance mechanisms reduce the ability of
38 a drug to disrupt its target, but do so at the expense of optimal physiological function (Lovmar
39 et al., 2009).

40 With few exceptions (Engelberg & Artman, 1964), resistance-causing alleles induce
41 physiological impairments in both drug-free and drug-containing environments, though
42 resistant strains may only suffer a strict competitive disadvantage (i.e. a slower growth rate)

43 against sensitive strains in drug-free conditions. A range of antibiotic concentrations therefore
44 exists within which drug-resistant strains have a selective advantage over their drug-
45 susceptible counterparts. Dosing drugs within this “resistance selection window” (also called
46 the “mutant selection window”) can allow for the proliferation of drug-resistant
47 subpopulations (Karl Drlica & Zhao, 2007; Gullberg et al., 2011; Yu, Baeder, Regoes, & Rolff,
48 2018). Recent advances in antimicrobial pharmacodynamics have leveraged the characteristics
49 of resistance selection windows to design dosing strategies that minimize the selection of
50 resistant pathogens without sacrificing treatment efficacy (Cui et al., 2006; Mohamed, Cars, &
51 Friberg, 2014; Yu et al., 2018).

52 The existence of resistance mutations that confer physiological impairments in both
53 drug-free and drug-containing environments implies that resistant strains face selective
54 pressures to evolve secondary mutations that alleviate these impairments, and that these
55 selective pressures exist even under continuous drug exposure (Loftie-Eaton et al., 2017;
56 Maisnier-Patin, Berg, Liljas, & Andersson, 2002). Secondary mutations can increase bacterial
57 fitness (through faster growth rates) in the absence of drugs, or they can confer elevated levels
58 of drug tolerance to preexisting resistant subpopulations (through attenuated drug-target
59 interactions, faster growth rates in the presence of drugs, or both). In the case of increased
60 bacterial fitness, secondary mutations enable drug-resistant mutants to compete against drug-
61 susceptible strains in resource-limited, antibiotic-free environments (Andersson & Hughes,
62 2010; Durão, Balbontín, & Gordo, 2018; Levin, Perrot, & Walker, 2000), and are implicated in
63 the spread of drug resistance across a wide range of timescales and clinical settings (Handel,
64 Regoes, & Antia, 2006). In the case of increased drug tolerance, secondary mutations can be
65 the underlying cause of treatment failure (Ahn et al., 2015; Merker et al., 2018). Elucidating the

66 dynamics of secondary mutation emergence during treatment is thus crucial for managing the
67 spread of resistance.

68 Since resistance mutations are frequently associated with fitness costs (Melnik et al.,
69 2015; Vogwill & MacLean, 2015) both *in vivo* (Majcherczyk, Barblan, Moreillon, & Entenza,
70 2008) and *in vitro* (Zhang, Sahin, McDermott, & Payot, 2006), studies on the resistance
71 selection window and on secondary adaptation have yielded valuable insights into the
72 emergence of drug-resistant bacteria during treatment. However, the design of optimal
73 resistance-mitigating drug dosing strategies remains challenging for two reasons. One
74 obstacle is that bacteria may acquire resistance through a multitude of mechanisms that
75 reduce antibiotic efficacy (Blair, Webber, Baylay, Ogbolu, & Piddock, 2015). These molecular
76 mechanisms may themselves influence the fitness landscape of resistance mutations (that is,
77 the relationship between the fitness cost of resistance and the selective advantage conferred
78 by the resistance mutation in drug-containing environments). A second challenge is that an
79 antibiotic's mechanism of action may affect the strength of selection for resistant strains over
80 drug-susceptible strains during treatment. One important feature of an antibiotic's cellular-
81 level mechanism of action is whether the drug controls bacterial populations by increasing
82 the rate of bacterial killing (i.e. bactericidal action) or by decreasing the rate of bacterial
83 replication (i.e. bacteriostatic action). Clinicians and researchers alike have argued that these
84 modes of antimicrobial action influence the dynamics of resistance selection (Frenoy &
85 Bonhoeffer, 2018; Stratton, 2003).

86 The design of resistance-mitigating antibiotic usage therefore depends on an
87 understanding of how a drug's mechanism of action, a pathogen's mechanism of resistance,
88 and the fitness landscape of resistance affect selection pressures during treatment. Tractable
89 and quantitative strategies for systematically exploring all of these factors have so far been

90 lacking. To address this gap, we developed a dynamical model that simulates the growth and
91 death of bacterial populations under antibiotic exposure using molecular-scale descriptions of
92 drug-target binding kinetics and cellular-scale descriptions of a drug’s mechanism of action.
93 In our model, higher numbers of inactivated drug-target complexes within a cell lead to
94 increases in antibiotic effect (either bacteriostatic, bactericidal, or a combination of the two).
95 The relationship between drug-target inactivation and antibiotic effect can take the shape of a
96 linear (i.e. gradual) or stepwise (i.e. sudden) function, as well as other intermediate forms
97 (**Supplementary Figure S1**). The model enables us to estimate critical pharmacodynamic
98 parameters from experimental datasets as effectively as with classical approaches (Regoes et
99 al., 2004), to simulate the fitness landscapes of resistance mutations against drugs with diverse
100 mechanisms of action, and to quantify the probability of secondary mutation emergence
101 within resistant subpopulations of bacteria during treatment.

102 We find that bacteria with resistance mechanisms that confer even modest reductions
103 in drug-target binding affinity can incur strikingly high (80-99%) fitness costs while still
104 maintaining higher drug tolerances than their susceptible counterparts, regardless of the
105 antibiotic’s mechanism of action. We also find that drugs with stepwise effects on bacterial
106 growth and death have narrower resistance selection windows than do drugs with linear
107 effects. However, our model suggests that whether a drug acts primarily through bactericidal
108 or bacteriostatic action has comparatively little influence on the strength of resistance
109 selection during treatment. We further demonstrate that, even with aggressive treatment
110 regimens, heterogeneous drug-target occupancy within a population enables fitness-impaired
111 resistant strains to develop secondary mutations that can lead to treatment failure. Our work
112 cautions that fitness costs may not limit the emergence of resistant strains that evolve through
113 reductions in drug-target binding affinity. We propose the “secondary mutant selection

114 window” as a novel pharmacodynamic characteristic of a drug that should be assessed
115 alongside other classic parameters such as the MIC and the resistance selection window when
116 designing robust resistance-mitigating antibiotic dosing strategies.

117

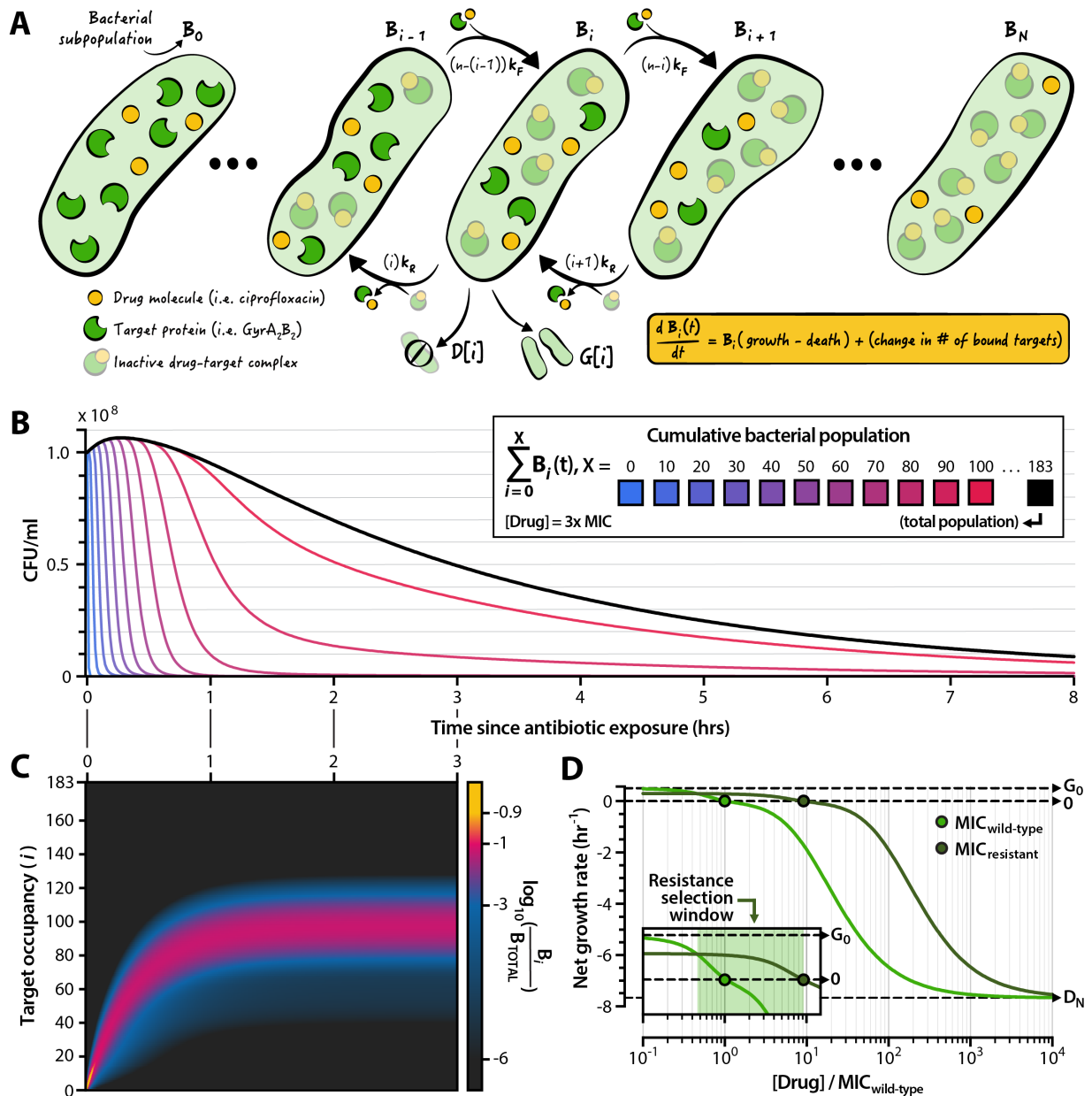
118 **Results**

119 *A model that links bacterial population dynamics with molecular mechanisms of antibiotic drug action*

120 We developed a linear dynamical model to describe the effect of a constant concentration of
121 drug on the growth and death rates of a bacterial population (**Figure 1A**) (see **Methods, Model**
122 *formulation and analysis* for a mathematical description of the model). We assume that each
123 bacterial cell in the population carries an identical number N of intracellular proteins that the
124 drug targets for inactivation. Drug molecules inactivate target proteins by binding to them
125 with a rate k_F and can dissociate from the target with a rate k_R . The affinity K_D of the drug is
126 thus the ratio of off-rate to on-rate, $K_D = k_R/k_F$. The model assumes that the growth and death
127 rates of a bacterial cell depend on its drug-target occupancy (that is, the number of inactivated
128 drug-target complexes it contains) (Clarelli et al., 2019; Wiesch et al., 2015). We denote drug-
129 target occupancy with the index i , which ranges from 0 to N . Cells harboring successively
130 larger numbers of inactivated drug-target complexes have successively faster death rates
131 and/or slower growth rates, depending on the mechanism of action of the drug (see **Results,**
132 *Classification of drug action*). We thus define the growth rate ($G[i]$) and death rate ($D[i]$) of each
133 subpopulation as discrete monotonic functions of drug-target occupancy. In practice, $G[i]$ and
134 $D[i]$ take the form of constrained logistic functions each controlled by a steepness and
135 inflection point parameter, allowing us to define quasi-linear, quasi-stepwise, quasi-
136 exponential, and sigmoid curves (**Supplementary Figure S1**).

137

138



139
140

141 **Figure 1 – Features of a model that links bacterial population dynamics with the cellular**
 142 **mechanisms of antibiotic drug action.** (A) Illustration of the model. We consider a
 143 population B_i of bacterial cells harboring i inactive drug-target complexes. The change in the
 144 size of B_i is a function of cellular growth and death rates (each of which is determined by the
 145 value of i), and of the molecular kinetics of the drug binding and unbinding to its protein
 146 target. The total bacterial population is given by the sum $B_0 + B_1 + \dots + B_{N-1} + B_N$, where N is the
 147 number of drug targets per cell. (B) Dynamics of a bacterial population exposed to a drug dose
 148 above the minimum inhibitory concentration (MIC). The black line represents the total
 149 bacterial population; shaded lines represent subpopulations with x and fewer inactivated
 150 drug-target complexes. (C) Proportion of the bacterial subpopulation B_i as a share of total

151 population for the first three hours of the curve shown in panel (B). (D) Pharmacodynamic
152 curves derived from the model for a wild-type (light green) and drug-resistant (dark green)
153 bacterial strain. The MIC is denoted as the drug concentration at which the net bacterial
154 growth rate is zero. Inset: the resistance selection window (green shading) is given by the drug
155 concentration range within which the drug-resistant strain exhibits a higher—but still
156 positive—net growth rate compared to the wild-type strain. G_o denotes the growth rate of the
157 wild-type strain in the absence of antibiotic (i.e. the growth rate for subpopulation B_o). D_N
158 denotes the maximum death rate of bacterial strains when all N cellular targets are inactivated
159 (i.e. the death rate of subpopulation B_N).

161 The model tracks the growth and death of all $N+1$ bacterial subpopulations, each
162 denoted B_i , over time (Figure 1B). Drug concentration determines the net growth rate of the
163 entire bacterial population (Supplementary Figure S2). In the absence of drug, the population
164 grows exponentially at a rate equal to the difference between the drug-free growth and death
165 rates (G_o and D_o , respectively). When drug is present, the composition of bacterial
166 subpopulations asymptotes towards a steady state after a transient phase during which drug
167 molecules bind to their targets (Figure 1C). At steady state, the relative composition of
168 bacterial subpopulations does not depend on the total size of the population.

169 We can calculate the MIC of a drug directly from model parameters (see **Methods**,
170 *Calculation of the minimum inhibitory concentration*), and we can simulate clinically observed
171 drug resistance mutations by modulating the parameters of the model that influence the value
172 of the MIC. Changes in the binding kinetics of the drug (i.e. k_F and k_R) simulate target
173 modification mutations that decrease the affinity of an antibiotic molecule to a cellular
174 protein (Billal, Feng, Leprohon, Légaré, & Ouellette, 2011; Everett, Jin, Ricci, & Piddock, 1996;
175 Gao et al., 2010). Changes to the value of N represent changes in the number of protein targets
176 per cell, equivalent to target up- or downregulation (Brochet, Couvé, Zouine, Poyart, & Glaser,
177 2008; Palmer, Chait, & Kishony, 2018; Palmer & Kishony, 2014). We assume that fitness costs
178 associated with resistance alleles take the form of reduced growth rates, and we simulate this
179 cost by reducing the drug-free growth rate of resistant strains by a factor c_R such that the

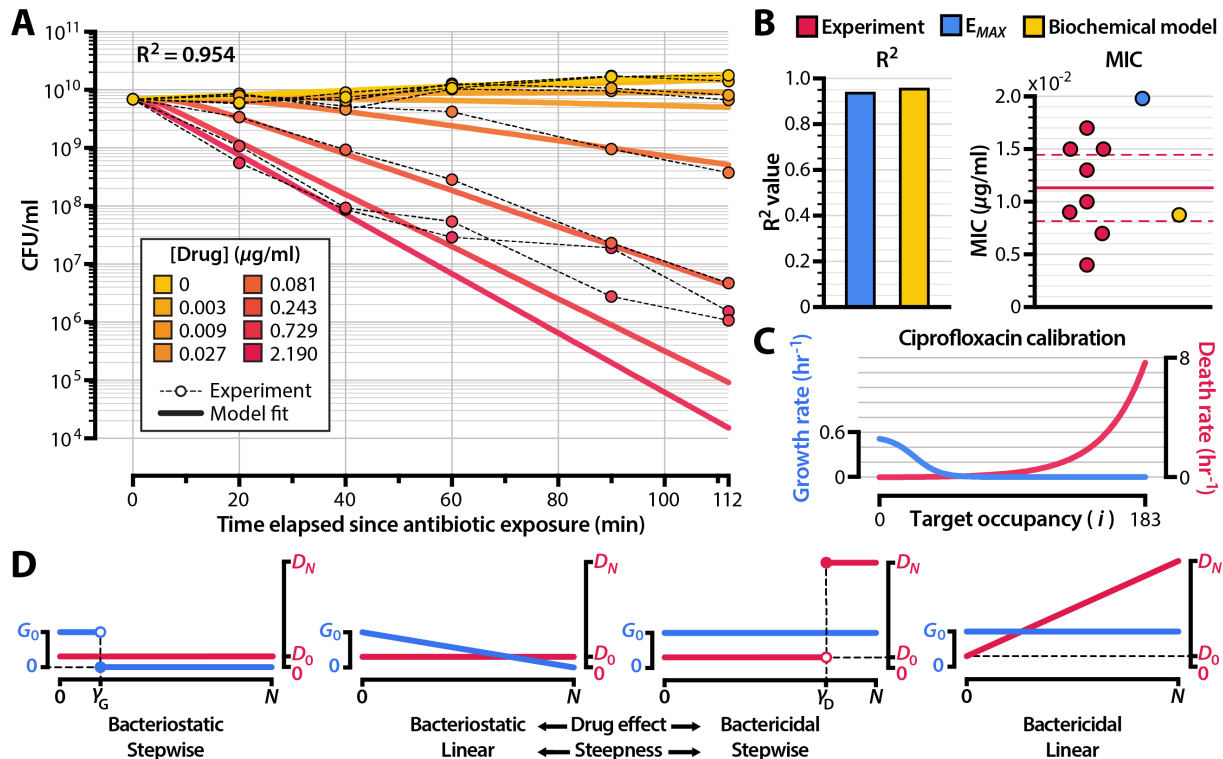
180 maximum growth rate of a resistant strain ($G_{o,RES}$) relative to that of a wild-type strain is $G_{o,RES}$
181 = $G_o(1-c_R)$. When c_R ranges from 0 (no cost) to 1 (no growth whatsoever), the resistant strain
182 exhibits a slower growth rate relative to that of the wild-type. If c_R is negative, the resistant
183 strain exhibits a faster drug-free growth rate than does the wild-type strain, as has been
184 observed in rare cases with some fluoroquinolone-resistant *Escherichia coli* isolates (Lindgren,
185 Marcusson, Sandvang, Frimodt-Møller, & Hughes, 2005). The model also enables us to
186 generate pharmacodynamic curves by calculating the net growth rates of simulated bacterial
187 populations over a range of drug concentrations (**Figure 1D**). The resistance selection window
188 constitutes the range of drug concentrations over which a drug-resistant mutant strain has a
189 higher but strictly positive net growth rate relative to that of its wild-type counterpart (**Figure**
190 **1D**, inset).

191

192 *Inferring cellular mechanisms of antibiotic action from population-scale data*

193 To test the utility of our biochemical model for gaining cellular-scale insights into
194 antimicrobial drug mechanisms from population-scale experiments, we calibrated our model
195 to a family of time-kill curves of the gram-negative bacterium *Escherichia coli* challenged to
196 ciprofloxacin, a fluoroquinolone first brought to market in 1987. Ciprofloxacin has two known
197 molecular targets in bacteria, both of which are heterotetrameric type-II topoisomerases: the
198 DNA gyrase complex ($GyrA_2B_2$) and DNA topoisomerase IV ($ParC_2E_2$). However, ciprofloxacin
199 preferentially binds to the $GyrA_2B_2$ complex in gram-negative bacteria (Karl Drlica, Malik,
200 Kerns, & Zhao, 2008). We used a mass-spectrometry based estimate for the number of
201 $GyrA_2B_2$ complexes per *E. coli* cell ($N \sim 183$) as the number of drug targets within each
202 bacterium (Wiśniewski & Rakus, 2014).

203 We implemented an adaptive simulated annealing algorithm to calibrate the
 204 parameters of our model to an experimental dataset of ciprofloxacin time-kill curves
 205 (Methods, Model calibration via simulated annealing). We performed 249 independent
 206 parameterizations using the algorithm and selected the parameter set that yielded the lowest
 207 objective function value (Figure 2A, Table 1, Supplementary Figure S3). Bacterial persistence
 208 (Dörr, Lewis, & Vulić, 2009; Harms, Maisonneuve, & Gerdes, 2016) likely plays a role in the
 209 slower-than-expected population decline that we observe experimentally at high drug
 210 concentrations. At antibiotic doses below those that elicit persistence, the calibrated model
 211 accurately recapitulates the pharmacodynamic curve derived from experimental data
 212 (Supplementary Figure S4).
 213



214
 215

216 **Figure 2 – Calibrating the model to experimental data reveals underlying mechanisms of**
 217 **drug action.** (A) Comparison between calibrated biochemical model (solid lines) and
 218 experimental data (Supporting Data File 1) represent

219 time-kill curves of *Escherichia coli* exposed to ciprofloxacin. (B) Comparison of calibrated
 220 biochemical model the E_{MAX} pharmacodynamic model (Regoes et al., 2004). We fit the E_{MAX}
 221 model to the same experimental dataset shown in panel (A) and compared correlation
 222 coefficients and MICs. Red points in the MIC panel denote experimentally-measured
 223 ciprofloxacin MICs for *E. coli* strains isolated prior to the widespread emergence of quinolone
 224 resistance (see **Supporting Data File 2**). The solid horizontal line represents the mean of
 225 experimental measurements, and the dashed lines indicate the 95% confidence interval. (C)
 226 Cellular growth and death rates as a function of ciprofloxacin-GyrA₂B₂ complex number (i) for
 227 the model calibrated to the experimental data shown in panel (A). (D) Four extreme schemes
 228 of drug action resulting from two characteristics (activity and steepness) of a drug's effect on
 229 growth and death rates as a function of drug-target occupancy. **Supplementary Figure S5**
 230 shows the simulated bacterial kill curves for these schemes at 4x MIC.
 231

Model parameters				
Name	Description	Value	Units	Source
N	Number of target proteins per cell (i.e. GyrA ₂ B ₂ copy number)	183	cell ⁻¹	(Wiśniewski & Rakus, 2014)
G_0	Bacterial growth rate in the absence of drug	0.526	hr ⁻¹	Model calibration
D_0	Bacterial death rate in the absence of drug	5.40×10^{-3}	hr ⁻¹	(Wang et al., 2010)
D_N	Bacterial death rate in saturating concentrations of drug	7.53	hr ⁻¹	Model calibration
k_F	Drug-target binding rate	5.23×10^3	M ⁻¹ sec ⁻¹	Model calibration
k_R	Drug-target unbinding rate	3.17×10^{-4}	sec ⁻¹	Model calibration
α_G	Steepness of growth rate function $G[i]$	16.8	# drug-target complexes ⁻¹	Model calibration
α_D	Steepness of death rate function $D[i]$	7.29	# drug-target complexes ⁻¹	Model calibration
γ_G	Inflection point of growth rate function $G[i]$	24.9	# drug-target complexes	Model calibration
γ_D	Inflection point of death rate function $D[i]$	359	# drug-target complexes	Model calibration
B_0	Initial size of bacterial population at the start of drug treatment	6.88×10^9	cell ml ⁻¹	Model calibration
μ_R	Mutation rate for drug resistance emergence	2.00×10^{-7}	cell ⁻¹ division ⁻¹	(Martinez & Baquero, 2000; Schulz zur Wiesch, Engelstädter, & Bonhoeffer, 2010)
μ_C	Mutation rate for emergence of secondary mutations in resistant strains	2.00×10^{-6}	cell ⁻¹ division ⁻¹	(Martinez & Baquero, 2000; Schulz zur Wiesch et al., 2010)
c_R	Cost of resistance mutation, such that the antibiotic-free growth rate of a resistant mutant is $G_0(1 - c_R)$	0.25	Non-dimensional	(Gagneux et al., 2006)

232
 233 **Table 1 – Model parameters.** We obtained the values of k_F , k_R , α_G , α_D , γ_G , γ_D , and B_0 by
 234 calibrating the model to experimental data (Figure 2). We inferred antibiotic-free growth rate
 235 and antibiotic-saturated death rate (G_0 and D_N) by fitting an exponential curve to
 236 ciprofloxacin kill curves using 0 and 2.19 µg/ml of drug, respectively (**Supplementary Figure**
 237 **SII**). We use a constrained logistic function to model the growth and death rates of bacterial

238 cells as a function of bound target number, where α controls the steepness of the logistic
239 function and γ controls the inflection point of the logistic function (**Supplementary Figure**
240 **S1**). Parameters not obtained from model calibrations to experimental data were retrieved
241 from the literature. For the bacterial death rate in the absence of drug (D_0), we used the mean
242 of death rates reported in Wang et al., 2010.
243

244 We compared our biochemical model's ability to capture critical pharmacodynamic
245 characteristics of a drug against that of an E_{MAX} model (Regoes et al., 2004). The E_{MAX} approach
246 describes net bacterial growth rate directly as a function of drug concentration and does not
247 accommodate molecular descriptions of drug-target interactions. Such models have been
248 used extensively to estimate pharmacodynamic parameters, to design drug dosing regimens,
249 and to predict the strength of resistance selection at nonzero drug concentrations. Our
250 formulation delivers performance comparable to that of the E_{MAX} model for fitting
251 experimental time-kill curves (**Figure 2B**, left panel) and more accurately estimates MIC
252 (which we determined to be $8.9 \times 10^{-3} \mu\text{g/ml}$ for ciprofloxacin) from these data (**Figure 2B**, right
253 panel). This demonstrates the validity of our approach for deriving pharmacodynamic
254 insights similar to what an E_{MAX} model provides.

255 Our model furthermore offers capabilities that the E_{MAX} approach lacks, including the
256 ability to estimate molecular kinetic parameters of drug-target binding from population-scale
257 data. To test the robustness of these estimates, we analyzed the K_D values for ciprofloxacin
258 binding to *E. coli* GyrA₂B₂ generated for the 249 independent parameterizations described
259 above. The best 90% of all calibrations (that is, the 224 fits with the lowest objective function
260 values) consistently converged upon a narrow range of affinity values (95% confidence
261 interval: 7.2×10^{-8} to 1.6×10^{-7} M) (**Supporting Data File 3**). Our estimates lie within the range of
262 K_D values of ciprofloxacin for *E. coli* GyrA₂B₂ reported from experimental measurements,
263 which span from 3.2×10^{-8} to 3.0×10^{-6} M (Jungkind & American Society for Microbiology

264 Eastern Pennsylvania, 1995; Kampranis & Maxwell, 1998; Shen & Pernet, 1985; Siporin, Heifetz,
265 & Domagala, 1990).

266

267 *Classification of antibiotic action*

268 Another unique feature of our approach is the ability to describe bacterial growth and death
269 rates as a function of drug-target occupancy. For ciprofloxacin, the calibrated model predicts
270 three regimes of bacterial subpopulation dynamics in relation to GyrA₂B₂ inactivation: a
271 growth regime in which bacterial replication dominates among subpopulations with low
272 numbers of inactivated targets, a stalling regime for intermediate numbers of drug-target
273 complexes in which neither growth nor death is appreciable, and a killing regime at high
274 numbers of inactivated targets in which bacterial death increases quasi-exponentially (**Figure**
275 **2C**). The forms of $G[i]$ and $D[i]$ that we obtain here suggest that ciprofloxacin has a
276 multimodal mechanism of action, a result consistent with prior experimental studies (K.
277 Drlica, 1999; Karl Drlica et al., 2008; Silva, Lourenço, Queiroz, & Domingues, 2011). The drug
278 stalls cellular replication at intermediate target occupancies and induces killing only at higher
279 doses. Like many antibiotics, ciprofloxacin thus exhibits both bactericidal and bacteriostatic
280 effects on microbial populations (Pankey & Sabath, 2004; Silva et al., 2011). Our biochemical
281 model represents this explicitly.

282 Most drugs nonetheless demonstrate a greater degree of bactericidal or bacteriostatic
283 activity at clinically relevant doses (Nemeth, Oesch, & Kuster, 2015), and we hypothesized that
284 the ability of a drug to stall growth or to accelerate death may affect the selection for resistant
285 strains and the emergence of secondary mutations. We also suspected that the relationship
286 between drug-target occupancy and antibiotic effect—reflected in the steepness of the $G[i]$
287 and $D[i]$ functions—could further shape the dynamics of resistance selection.

288 These two characteristics (bactericidal versus bacteriostatic activity and drug effect
289 steepness) represent two general dimensions along which a drug's mechanism of action can
290 affect the growth and death of bacterial populations. Four extreme cases of drug action thus
291 exist (**Figure 2D**). In the case of a purely bacteriostatic antibiotic, death rates are a constant
292 function of inactivated drug-target complex number (that is, $D[i] = D_o$ for all values of i). For a
293 purely bactericidal antibiotic, the growth rate of all bacterial subpopulations remains constant
294 ($G[i] = G_o$ for all values of i). The steepness of the drug effect is reflected in the form of the
295 function $D[i]$ for bactericidal antibiotics and $G[i]$ for bacteriostatic antibiotics (**Supplementary**
296 **Figure S1**). We defined linear and stepwise onset of action as our two extremes, as other
297 monotonic forms are intermediate cases of these curves.

298

299 *The opposing effects of increased drug resistance and decreased cellular fitness*

300 Mutations that confer resistance against antibiotics often come at the cost of reduced growth
301 rates compared to those of drug-susceptible strains (Andersson & Hughes, 2010; Melnyk et al.,
302 2015). The balance of replication and death determines bacterial net growth both in the
303 absence and in the presence of antibiotics, and very high fitness costs associated with
304 resistance can prevent bacterial viability at any drug concentration (Björkman, Nagaev, Berg,
305 Hughes, & Andersson, 2000). We sought to investigate the quantitative basis for the trade-off
306 between drug resistance and cellular growth and to investigate how the drug mechanisms
307 defined above influence the range of permissible fitness costs that a drug-resistant mutant can
308 incur while still maintaining a drug susceptibility that is lower than that of a wild-type strain.
309 In the simplest case of the model, where the number of target molecules per cell is 1, the
310 expression for the MIC captures the opposing effects of drug resistance and cellular growth
311 (see **Methods**, *Calculation of minimum inhibitory concentration* for derivation):

312 [Equation 1]

313
$$\text{MIC} = \frac{(k_R + D_N)}{k_F D_N} G_0$$

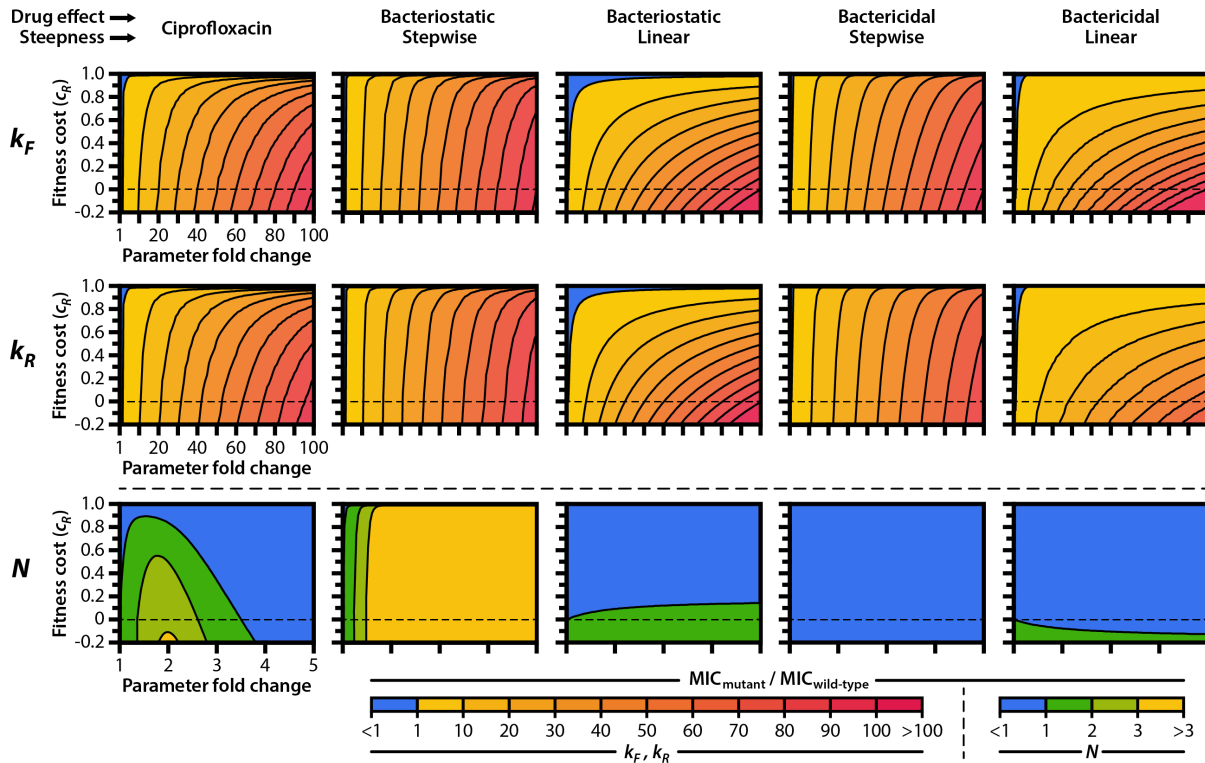
314 The MIC increases with reductions of the on-rate kinetics of drug-target binding (k_F) and with
315 increases in the off-rate kinetics of drug-target binding (k_R), but decreases with fitness costs
316 that manifest as reductions in the drug-free growth rate (G_0). These proportionalities hold for
317 any number N of drug targets.

318 We modeled the opposing effects of biochemical changes that reduce drug
319 susceptibility (i.e. altered drug-target binding kinetics or target upregulation) and the fitness
320 costs of these biochemical changes. We considered a set of five antibiotics with an identical
321 protein target and identical molecular kinetic parameters (that is, the target number N , the
322 drug-target on-rate k_F , and the drug-target off-rate k_R are constant for the wild-type strain)
323 (Supplementary Table S1, Supplementary Figure S5). One antibiotic in the set features
324 growth and death dynamics derived from the model calibration to ciprofloxacin time-kill
325 curve data (Figure 2C). The other four antibiotics are hypothetical and feature growth and
326 death dynamics that represent four extremes of antibiotic action (Figure 2D). We simulated
327 mutant strains of *E. coli* that acquire drug resistance phenotypes either through changes in the
328 molecular kinetics of drug binding (k_F or k_R) or by increasing the copy number N of the drug's
329 cellular protein target. Each of these resistance mechanisms has been observed in clinical
330 isolates of drug-resistant, gram-negative bacteria (Blair et al., 2015; Melnyk et al., 2015;
331 Redgrave, Sutton, Webber, & Piddock, 2014). We then simulated fitness costs associated with
332 the resistance mutation and calculated the mutant strain's MIC relative to that of the wild-
333 type strain.

334 For resistance acquired through changes in the kinetics of drug-target binding (k_F and
335 k_R), we found that mutants can tolerate strikingly high (80-99%) fitness costs while still

336 maintaining an MIC that is greater than that of the drug-susceptible wild-type (**Figure 3**, top
337 and middle rows). This permissibility of fitness costs exists for all five of the drug mechanisms
338 we simulated, although drugs that act with linear effects (Bacteriostatic/Linear and
339 Bactericidal/Linear) have a narrower range of permissible fitness costs than do drugs that act
340 with stepwise effects. For all drug mechanisms, mutant strains make larger gains in MIC by
341 decreasing the on-rate kinetics of drug-target binding (k_F) than they do by increasing the off-
342 rate kinetics of drug-target binding (k_R) by the same amount (**Supplementary Figure S6**). That
343 is, mutations that lead to the same change in drug-target affinity (as quantified by the
344 dissociation constant $K_D = k_R/k_F$) through different changes in the on- and off-rate binding
345 kinetics do not necessarily have the same range of permissible fitness costs. This has
346 biological significance—limiting the opportunity for a drug to bind to its target, thereby
347 preventing the drug from actuating its effects on cellular growth and death, should lead to
348 lower drug susceptibilities than would accelerating the rate at which an already-formed drug-
349 target complex disassociates. The difference in the fitness effects of mutations that modify k_F
350 and k_R is especially pronounced for bactericidal drugs that elicit linear increases in cellular
351 death (Bactericidal/Linear).
352

353



354
355

356 **Figure 3 – Drug mechanism influences the fitness landscapes of resistance mutations.** We
357 calculated the MIC, expressed as a fold-change relative to the MIC of the wild-type, for
358 mutant strains carrying (top row) drug targets with reduced binding kinetics (k_F), (middle row)
359 drug targets with accelerated unbinding kinetics (k_R), or (bottom row) increased numbers of
360 drug target molecules (N). Mutant strains also carry fitness costs, expressed as a fractional
361 reduction in drug-free growth rate relative to wild-type. When modulating the number of
362 drug target molecules N (bottom row), we assumed that cells require a fixed number of active
363 protein targets to grow at a normal rate and that cellular killing is induced when a fixed
364 number of inactive drug-target complexes form within a cell. Thus, the inflection point for the
365 growth rate function (γ_G) changes concomitantly with N such that $N \cdot \gamma_G$ remains constant,
366 while the inflection point for the death rate function (γ_D) remains constant (see
367 **Supplementary Figure S1** for illustrations of the effects of γ_G and γ_D on bacterial growth and
368 death rates).

369

370 Ciprofloxacin exhibits a bactericidal effect by permitting GyrA₂B₂-mediated cleavage
371 of DNA but preventing DNA re-ligation, resulting in widespread and eventually
372 insurmountable chromosome fragmentation (Karl Drlica et al., 2008; Pan, Yague, & Fisher,
373 2001). When simulating the overexpression of target proteins in resistant cells (**Figure 3,**

374 bottom row) we therefore assumed that bacterial killing is induced when a fixed number of
375 inactivated drug-target molecules form within a cell (that is, we assume a toxicity threshold
376 whereby γ_D remains constant with changing N). Conversely, we assumed that a resistant cell
377 requires a fixed number of active, non-complexed target proteins in order to maintain its
378 maximum growth rate (that is, a survival threshold). γ_G thus changes in step with N such that
379 $N-\gamma_G$ remains constant. We made these same assumptions for the four hypothetical
380 antibiotics.

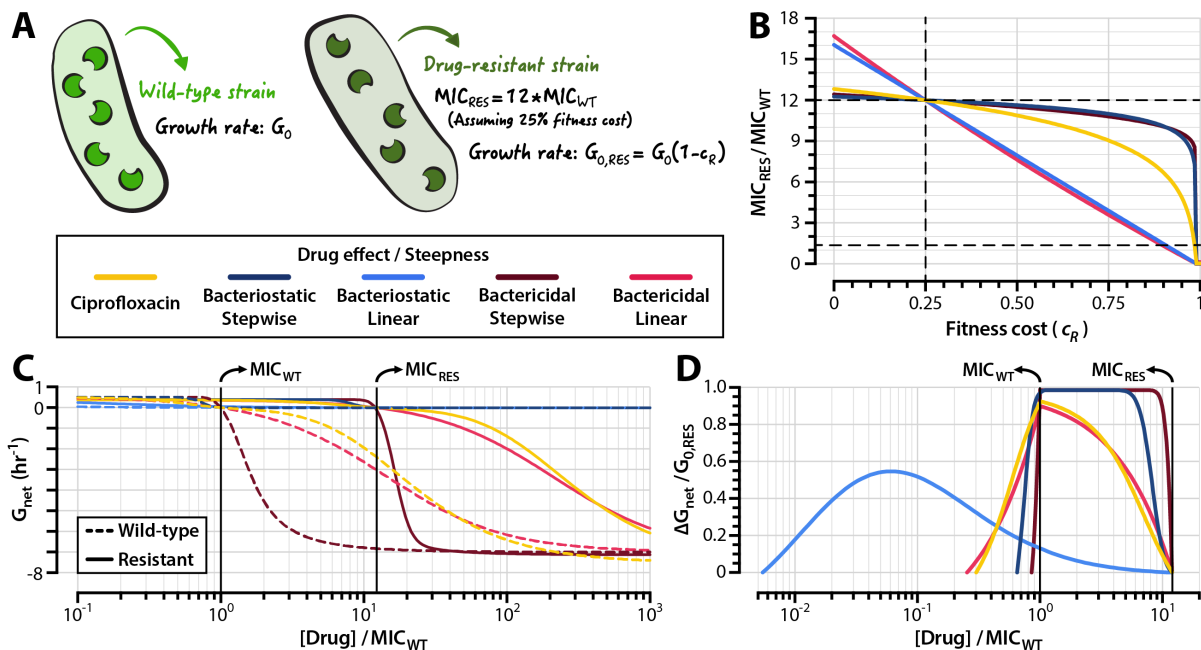
381 We found that target overexpression has a diversity of effects on resistance that
382 depend on the mechanism of action of the drug. For ciprofloxacin and its multimodal effects
383 on growth and death, small increases in target number can lead to modest increases in MIC,
384 even when the resistant cell faces large fitness costs as a result of GyrA₂B₂ overexpression.
385 However, larger increases in target number lead to reductions in MIC. This result is consistent
386 with experimental studies on target amplification, in which the overexpression of *gyrAB* in *E.*
387 *coli* resulted in increased susceptibility to ciprofloxacin (Palmer & Kishony, 2014). Target
388 overexpression leads to substantial gains in resistance against bacteriostatic drugs that exhibit
389 stepwise effects, even at very high fitness costs. The effect of target overexpression on drug
390 resistance is negligible for bactericidal drugs and for bacteriostatic drugs with a linear effect
391 on growth stalling.

392

393 *Drug mechanism shapes the resistance selection window*

394 To understand how a drug's mechanism of action affects the propensity to select for resistance
395 during treatment, we simulated the pharmacodynamics of wild-type and drug-resistant
396 strains challenged to each of the five drugs in the set outlined above. MICs for clinical isolates
397 of ciprofloxacin-resistant *E. coli* strains with single point mutations in GyrA, which may

398 reduce the affinity of ciprofloxacin to GyrA₂B₂, range from 10 to 16 times greater than the MIC
 399 of a drug-susceptible wild-type (Everett et al., 1996; Morgan-Linnell & Zechiedrich, 2007;
 400 Piddock, 1999; Redgrave et al., 2014). Data on the fitness costs associated with mutant GyrA-
 401 mediated ciprofloxacin resistance in *E. coli* are sparse, but studies of rifampicin-resistant
 402 clinical isolates of *Mycobacterium tuberculosis* with point mutations in the *rpoB* gene have
 403 suggested that a 20-30% reduction in growth rate is approximately the maximum fitness cost
 404 that drug-resistant mutants can incur before facing extinction in competitive drug-free
 405 environments (Gagneux et al., 2006). To model drug-resistant strains, we therefore scaled k_F
 406 and k_R such that the MIC of the resistant strain is 12 times that of its drug-susceptible
 407 counterpart given a 25% fitness cost ($c_R = 0.25$) (Figure 4A).
 408



409
 410
 411 **Figure 4 – The propensity to select for resistant mutants depends on drug mechanism. (A)**
 412 We modeled wild-type strains using the parameters obtained from the calibration detailed in
 413 **Figure 2. (B) Relationship between MICs of resistant strains (expressed as multiples of**
 414 **MIC_{WT}) and fitness cost of resistance. Horizontal dashed lines indicate the MICs of the wild-**
 415 **type and resistant strains described in panel (A); the vertical dashed line indicates the fitness**
 416 **cost at which all resistant strains have the same fold-increase in MIC relative to that of wild-**

417 type ($c_R = 0.25$). (C) Pharmacodynamic curves for the wild-type and resistant strains described
418 in panel (A). (D) Resistance selection windows for drug-resistant strains. The fitness advantage
419 of resistant strains over wild-type strains is shown within the drug concentration range in
420 which the resistant strain has a positive net growth rate that is larger than that of the wild-
421 type. The fitness advantage is expressed as a proportion of the resistant strain's growth rate in
422 the absence of drug ($G_{o,RES}$).
423

424 A nearly linear relationship exists between drug resistance and fitness cost for strains
425 resistant to drugs with a linear effect on growth or death (**Figure 4B**, Bacteriostatic/Linear and
426 Bactericidal/Linear). By contrast, drugs with stepwise effects on growth and killing
427 (Bacteriostatic/Stepwise and Bactericidal/Stepwise) exhibit only modest reductions in MIC
428 until they incur very high (>90%) fitness costs. We determined resistance selection windows
429 for strains resistant to the five drugs in our set by simulating pharmacodynamic curves for
430 wild-type and resistant strains (**Figure 4C**). To quantify the magnitudes of selection for
431 resistant strains, we calculated the difference in net growth rates between wild-type and
432 susceptible strains over the concentration range that defines the resistance selection window
433 for each drug (**Figure 4D**). For linear-effect bacteriostatic drugs (Bacteriostatic/Linear), we
434 found that the resistance selection window begins at drug concentrations as low as 200x
435 below the MIC of the susceptible strain. Drugs with stepwise effects on growth or killing
436 (Bacteriostatic/Stepwise and Bactericidal/Stepwise) have narrower resistance selection
437 windows than their counterparts with more linear activity profiles.

438 Consistent with prior studies on the pharmacodynamic profiles of antimicrobial agents
439 (Mohamed et al., 2014; Nielsen & Friberg, 2013; Yu et al., 2018), we find that the size of the
440 resistance selection window is associated with the steepness of a drug's pharmacodynamic
441 curve. Given a cellular effect (i.e. bacteriostatic or bactericidal), drugs with steeper
442 pharmacodynamic curves tend to have narrower selection windows (**Supplementary Figure**
443 **S7**). However, we also find that strains resistant to drugs with narrower resistance selection

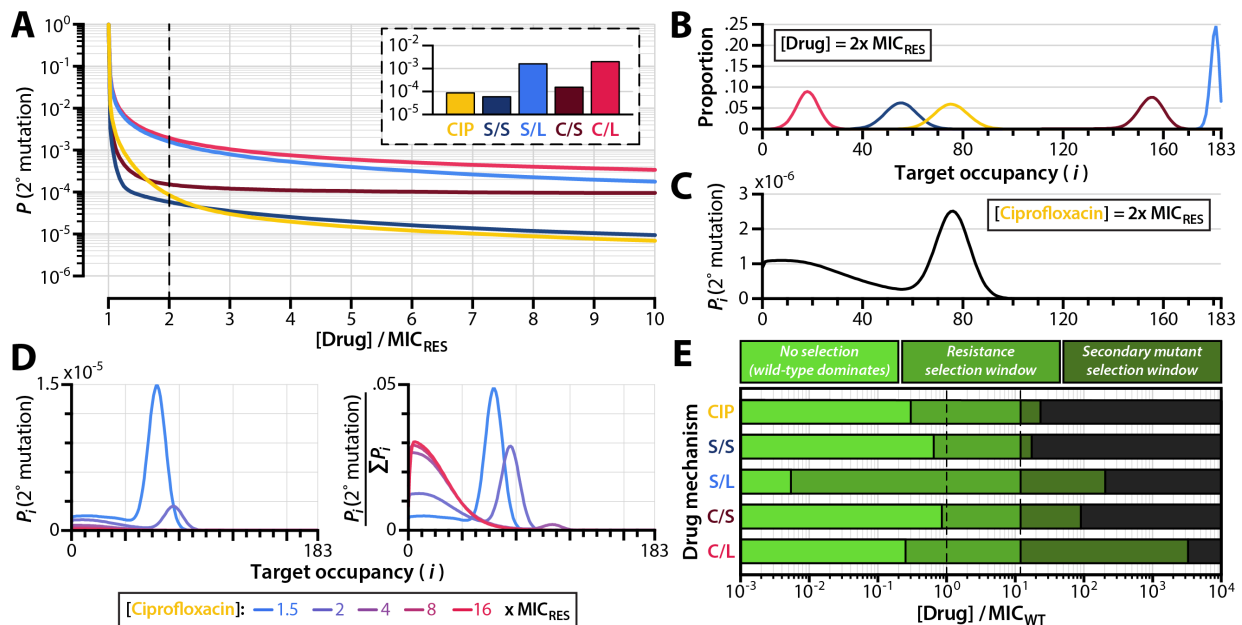
444 windows have higher net growth rates within the resistance selection regime than do strains
445 resistant to drugs with wider resistance selection windows (**Figure 4D**). This finding has clear
446 clinical significance: drugs with steeper pharmacodynamic profiles feature relatively small
447 concentration ranges that select for resistance, but the negative consequences of dosing within
448 the resistance selection window are higher for these drugs.

449
450 *The secondary mutant selection window is narrower for antibiotics with stepwise effects on growth*
451 *and death*

452 The genotypic space for mutations that confer resistance to antibiotics by modifying the
453 binding kinetics of a drug to its target, such as those described in **Figure 4**, is typically highly
454 constrained (Levin et al., 2000; Palmer & Kishony, 2013). This is because a return to a drug-
455 susceptible state requires reversion of the specific genetic changes that conferred resistance in
456 a bacterial population, whereas secondary mutation accumulation can involve a wider range
457 of genetic changes throughout the cell's metabolic network. Therefore, the probability that a
458 bacterial population evolves secondary mutations that compensate for the fitness costs of a
459 resistance mutation is often higher than the probability that a bacterial population will revert
460 to susceptibility in drug-free environments (Isalan et al., 2008; Maisnier-Patin et al., 2002).
461 During treatment, resistant bacterial populations may also accumulate secondary mutations
462 that further raise MIC. In order to understand how drug mechanism influences such
463 secondary adaptation, we simulated the emergence of secondary mutants from drug-resistant
464 subpopulations of a bacterial population faced with antibiotic challenge (**Supplementary**
465 **Figure S8; Methods, Simulating the emergence of secondary mutations**).

466 The probability of secondary mutation emergence is substantially higher for drugs
467 with linear effects on cellular growth and death than it is for drugs with stepwise effects

468 (Figure 5A). This holds true for both bactericidal and bacteriostatic agents. Counterintuitively,
 469 then, the suppression of secondary mutation emergence is not necessarily guaranteed by
 470 rapid killing as suggested by earlier studies (Lipsitch & Levin, 1997). Likewise, rapid
 471 attenuation of cell division does not halt the emergence of secondary mutations. We studied
 472 the basis for this result by investigating the steady-state target occupancy distributions of cells
 473 under antibiotic exposure. By accounting for the kinetics of drug-target binding, our
 474 biochemical model shows that target occupancy among cells follows a distribution and is not
 475 a single value even in otherwise clonal bacterial subpopulations (Figure 5B). This results in
 476 heterogeneous replication rates within the drug-resistant subpopulation (Supplementary
 477 Figure S9) that allow some bacteria to mutate. Classical population-dynamic models of
 478 antibiotic action (Lipsitch & Levin, 1997; Regoes et al., 2004), which assume that a drug affects
 479 the net growth rate of all cells equally, overlook this phenomenon.
 480



481
 482
 483 **Figure 5 – Emergence of secondary mutations among resistant subpopulations of infecting**
 484 **bacteria.** (A) Probability of a drug-resistant strain with secondary mutations emerging from
 485 an infecting bacterial population before the infection is cleared (i.e. before the total bacterial

486 population decreases to less than 1). The initial population size for this simulation is 10^9 cells.
487 Inset shows probabilities of secondary mutation emergence before infection clearance when
488 the drug concentration used is $2x$ MIC_{RES} . (B) Frequency distributions of inactive drug-target
489 complexes for drug-resistant subpopulations undergoing steady-state exponential decline at
490 $2x$ MIC_{RES} . (C) Probability of secondary mutant emergence from bacterial subpopulations
491 with i inactivated drug-target complexes, shown for ciprofloxacin dosed at $2x$ MIC_{RES} . (D)
492 Probability of secondary mutant emergence from bacterial subpopulations as a function of
493 drug dose, shown for ciprofloxacin dosed at $2x$ MIC_{RES} . Probabilities are shown as absolute
494 values (left panel) and as values normalized to the total probability of compensation for the
495 entire bacterial population over the course of treatment (right panel). (E) Resistance and
496 secondary mutant selection windows for different drug action mechanisms. The resistance
497 selection window (middle green) is defined as the drug concentration range over which a
498 drug-resistant strain has a growth advantage over wild-type. The secondary mutant selection
499 window (dark green) is defined as the drug concentration range over which the probability of
500 a resistant strain with secondary mutations emerging before infection clearance exceeds 10^{-4}
501 (see **Supplementary Figure S10** and **Methods, Simulating the emergence of secondary mutations**).
502 Dashed lines indicate the MICs of the wild-type and resistant strains. CIP: ciprofloxacin; S/S:
503 bacteriostatic/stepwise effect; S/L: bacteriostatic/linear effect; C/S: bactericidal/stepwise effect;
504 C/L: bactericidal/linear effect; MIC_{WT} : MIC of the wild-type strain; MIC_{RES} : MIC of the
505 resistant strain.
506

507 For ciprofloxacin doses only slightly above the MIC of the resistant strain ($[Drug] = 2x$
508 MIC_{RES}), we found that secondary mutations are most likely to emerge once the bacterial
509 population has reached a steady-state target occupancy distribution (**Figure 5C**). A
510 considerable probability of secondary mutation emergence nonetheless exists among
511 bacterial subpopulations with low numbers of inactivated drug-target complexes. These low-
512 occupancy subpopulations have faster growth rates and thus higher mutation rates. They are
513 also present in very large numbers during the initial stages of treatment, when drug molecules
514 are binding to their cellular targets and before the overall population begins to decline
515 (**Figure 1C**). We found that drug concentration influences the likelihood of a secondary
516 mutant arising from a steady-state or a low-occupancy subpopulation (**Figure 5D**). While the
517 overall probability of secondary mutation emergence decreases with higher drug dose (**Figure**
518 **5D**, left panel), the relative probability that a secondary mutation arises from a low-occupancy
519 population is greater for higher drug doses (**Figure 5D**, right panel). This implies that

520 secondary mutations are more likely to emerge very early during treatment when high drug
521 doses are used.

522 Prior studies have estimated that the probability of the existence of a fitness cost-free
523 bacterial pathogen prior to treatment ranges from 3×10^{-4} to 5×10^{-5} per infection (Colijn,
524 Cohen, Ganesh, & Murray, 2011). We sought to determine the range of drug concentrations
525 over which the likelihood of secondary mutation emergence during treatment is at least as
526 high as the likelihood for preexisting secondary resistance. We therefore determined the drug
527 concentration at which the probability of secondary mutation emergence before population
528 extinction equals 10^{-4} (that is, each treatment course has a 1 in 10,000 chance of giving rise to a
529 resistant strain bearing secondary mutations). We used this value as an upper boundary for
530 the “secondary mutant selection window,” the range of drug concentrations over which the
531 probability of the emergence of a drug-resistant bacterial strain with secondary mutations is
532 substantial (**Supplementary Figure S10**). The secondary mutant selection window extends the
533 range of drug concentrations defined by the resistance selection window over which drug-
534 resistant strains may be selected (**Figure 5E**).

535 As with the resistance selection window, we found that the size of the secondary
536 mutant selection window varies dramatically depending on a drug’s mechanism of action.
537 Drugs with linear effects on cellular growth and death have larger secondary mutant selection
538 windows than do drugs with stepwise effects on cellular growth and death. This is because for
539 drugs with stepwise effects, it is possible to shift the entire distribution of target occupancy to
540 a range where bacterial replication is virtually eliminated (or where bacterial death far
541 outweighs replication) across the entire population. With linear action, replication can still
542 occur even at high target occupancy, enabling the emergence of mutants. Drugs that fully
543 suppress cellular replication above MIC (i.e. Bacteriostatic/Stepwise) have small secondary

544 mutant selection windows, as the probability that additional mutations emerge over the
545 course of treatment is equal to the probability that a resistant strain with secondary mutations
546 emerges during the transient phase of drug-target binding immediately after treatment onset,
547 which lasts on the order of a few hours (**Figure 1C**).

548

549 **Discussion**

550 The increasing prevalence of first line- and multi-drug resistant bacteria (WHO, 2012, 2014)
551 signals the need for new antibiotics and robust drug dosing strategies that minimize the
552 emergence and spread of resistance (CDC, 2019). Despite this need, little is known about the
553 role that a drug's mechanism of action plays on the evolution of antibiotic resistance. We
554 studied the relationship between drug mechanism and drug resistance using a mathematical
555 model that connects bacterial population dynamics with molecular-scale descriptions of drug-
556 target binding kinetics (**Figure 1A**). Our biochemical model allows us to describe bacterial
557 replication and death as functions of drug-target occupancy, enables us to estimate molecular
558 kinetic parameters from population-scale data, and delivers performance on par with that of
559 classical pharmacodynamic models (**Figure 2B**).

560 We calibrate the model to an experimental dataset of ciprofloxacin time-kill curves
561 (**Figure 2A, Table 1**), and we show that drug-resistant strains can incur strikingly high fitness
562 costs associated with mutations that reduce drug-target binding kinetics (**Figure 3**). We find
563 that the relationship between drug-target inactivation and antibiotic effect (i.e. bacterial
564 killing, growth stalling, or both) exerts a strong influence on the strength of selection for
565 resistant strains during treatment, regardless of whether the drug is bactericidal or
566 bacteriostatic (**Figure 4D**). We also show that the molecular kinetics of drug-target binding
567 within cells results in heterogeneous replication rates among members of an otherwise

568 homogenous population (**Figure 5B**). This enables some drug-resistant strains to develop
569 secondary mutations that can further reduce drug susceptibility, increase resilience in drug-
570 free environments, and ultimately lead to treatment failure.

571 The clinical consequence of the frequently-observed trade-off between bacterial
572 fitness and drug resistance (Andersson & Hughes, 2010) is the existence of a resistance
573 selection window—a range of drug concentrations that selects for the propagation of drug-
574 resistant strains over their drug-susceptible counterparts (Karl Drlica & Zhao, 2007; Roberts et
575 al., 2008). It is important to note that numerous factors not captured by the resistance
576 selection window can contribute to resistance selection in clinical settings, most notably
577 ecological interactions between drug-susceptible strains, drug-resistant strains, and host
578 physiology (Day, Huijben, & Read, 2015). Our approach nonetheless enables us to isolate the
579 roles that a drug’s mechanism of action play in driving the emergence of resistance.

580 We show that the resistance selection window is narrower for drugs that exert their
581 effects on growth or death in a stepwise (i.e. sudden) manner, resulting in a steeper
582 pharmacodynamic curve (**Figure 4C-4D, Supplementary Figure S7**). This result is consistent
583 with other studies on the pharmacodynamics of antimicrobial agents, which have found that
584 the size of the resistance selection window is associated with the steepness of the
585 pharmacodynamic curve (Mohamed et al., 2014; Nielsen & Friberg, 2013; Yu et al., 2018). The
586 characteristics of antimicrobial agents that enable steeper pharmacodynamic curves
587 nonetheless remain poorly described. Models that capture the effects of antibiotic drugs on
588 multiple scales, such as that described in this study and elsewhere (Clarelli et al., 2019; Wiesch
589 et al., 2015), could serve as helpful tools for studying the interplay between a drug’s molecular
590 mechanism and its effect on bacterial population dynamics, enabling the design of new
591 antimicrobial agents with narrow resistance selection windows.

592 Mutations that alleviate the fitness costs associated with drug resistance and/or that
593 further raise a strain's MIC play a major role in driving the spread of antimicrobial resistance
594 across bacterial populations and clinical settings (Handel et al., 2006). Our study sheds
595 quantitative light on the mechanistic factors that govern the emergence of these secondary
596 mutations during treatment. We propose the use of the secondary mutant selection window
597 (**Supplementary Figure S10**) as a tool for illustrating the likelihood of further mutation
598 acquisition at nonzero drug concentrations. As with the size of the resistance selection
599 window, the size of the secondary mutant selection window varies greatly depending on the
600 mechanism of action of the antibiotic (**Figure 5E**). We stress that the secondary mutant
601 selection window does not necessarily indicate a region on the pharmacodynamic profile of a
602 drug over which the selection of a resistant strain with secondary mutations is favored. The
603 strength of selection depends on the physiological effect of the secondary mutation itself—
604 that is, whether the mutation accelerates growth rate, slows drug-target binding, or exerts a
605 multitude of other possible effects. Indeed, secondary mutations that act strictly by restoring
606 growth rates to wild-type levels lead only to modest (usually sublinear) increases in MIC
607 (**Figure 4B**), implying that strains with cost-free resistance phenotypes would still have MICs
608 well below the upper boundary for the secondary mutant selection windows shown in **Figure**
609 **5E**. Rather, the secondary mutant selection window defines the drug concentration range
610 within which the accumulation of secondary mutations is substantial and therefore clinically
611 significant.

612 Suppressing secondary mutation is crucial for reducing the survival of drug-resistant
613 mutants in antibiotic-free environments, where drug-resistant strains enter into direct
614 competition with other microbial organisms for limited resources (Andersson & Hughes, 2010;
615 Durão et al., 2018). We demonstrate that dosing drugs at or slightly above the MIC of a

616 resistant strain may not be sufficient for preventing the spread of resistance, and that—for
617 drugs with linear effects on bacterial growth and death as a function of drug-target
618 occupancy—there exist appreciable risks of selecting for secondary mutations even at doses
619 substantially above the MIC of the resistant strain. Reassessing the range of drug
620 concentrations that selects for resistant mutants as a composite of the resistance selection
621 window and the secondary mutant selection window (**Figure 5E, Supplementary Figure S10**)
622 could facilitate the design of drug dosing strategies that holistically mitigate the emergence
623 and spread of resistance.

624 Our study shows that both bactericidal and bacteriostatic drugs are capable of
625 exhibiting narrow resistance selection windows and low probabilities of secondary mutation
626 emergence in bacterial populations subjected to antibiotic treatment. This finding challenges
627 the long-accepted notion that bactericidal agents are superior to bacteriostatic agents in
628 suppressing the emergence of resistance during treatment (Stratton, 2003), and signals the
629 need to look beyond a drug’s ability to kill or stall bacterial replication to assess the risks of
630 resistance emergence. The relationship between drug-target inactivation and overall
631 antibiotic effect has a much stronger influence on the strength of resistance selection than
632 does the drug’s bacteriostatic or bactericidal activity (**Figure 4D**). The processes that may
633 dictate such a relationship for any given antibiotic nonetheless remain enigmatic. This
634 underscores the need for deeper experimental and theoretical research on the molecular
635 processes that govern the pharmacodynamics of antibiotic drugs.

636 The proper use of antibiotics in clinical and non-clinical settings constitutes a core
637 action for addressing the worldwide threat of antibiotic resistance (CDC, 2019). The
638 quantitative approach we present in this study may prove useful for identifying strategies that
639 manage the emergence of resistance to existing and future antimicrobial agents. We argue

640 that dosing regimens should account for a drug's resistance and secondary mutant selection
641 windows if they are to minimize the selection of resistance phenotypes during treatment. Our
642 findings suggest that even drugs with seemingly straightforward pharmacodynamic
643 classifications (i.e. bacteriostatic versus bactericidal action) can set bacterial populations on
644 complex and sometimes counterintuitive evolutionary trajectories with respect to resistance
645 selection. In the clinic, there exists little evidence that bactericidal antibiotics lead to more
646 favorable outcomes than do bacteriostatic antibiotics, especially for combatting
647 uncomplicated infections (Leekha, Terrell, & Edson, 2011; Pankey & Sabath, 2004). Yet it is
648 precisely in the treatment of uncomplicated, drug-susceptible infections that the greatest
649 gains are to be made in mitigating the emergence of resistance. Mechanistic models such as
650 that presented in this study can help to uncover clinically useful drug characteristics that
651 classical models may overlook. We envision a coupling of our quantitative approach with
652 high-throughput experimental platforms (Kulesa, Kehe, Hurtado, Tawde, & Blainey, 2018;
653 Schoepp et al., 2017) to aid in the development of new drugs with optimal pharmacodynamic
654 profiles and to accelerate the discovery of drug- and pathogen-specific dosing regimens that
655 minimize resistance emergence.

656

657 **Methods**

658 *Bacterial time-kill curve experiment*

659 We conducted time-kill curve experiments using *Escherichia coli* strain BW25113 (Coli Genetic
660 Stock Center #7636) (Datsenko & Wanner, 2000). We diluted overnight cultures of BW25113
661 1:1000 into pre-warmed lysogeny broth (LB) and grew cells to an optical density at 600nm
662 (OD₆₀₀) of 0.50. We then prepared a 1:3 dilution series of ciprofloxacin (highest concentration:
663 2.19 µg/ml) and added the antibiotics to bacterial cultures. We quantified bacterial population

664 sizes at regular (20-30 min) time intervals by plating a 1:10 dilution series of liquid culture onto
665 LB agar plates and counting colony forming units in technical triplicate. The bacterial kill
666 curve obtained at the highest ciprofloxacin concentration was used to determine the
667 maximum death rate (D_N) of bacterial cells, and a growth curve obtained using the same
668 protocol with the omission of ciprofloxacin was used to determine the maximum growth rate
669 (G_o) of cells in an antibiotic free environment (**Supplementary Figure S11**).

670

671 *Model formulation and analysis*

672 Our biochemical model constitutes a system of linear ordinary differential equations that
673 describe how successive numbers of inactivated drug-target complexes affect bacterial
674 replication and death. We consider a population of initial size B_o of phenotypically
675 homogenous and clonal bacteria exposed to a constant concentration C_o of drug. When no
676 drug is present, bacterial cells replicate at a rate G_o and die at a rate D_o . All cells have an
677 identical number N of proteins that drug molecules target for inactivation. We assume first-
678 order kinetics for drug-target binding: drug molecules bind to cellular protein targets within
679 cells, thereby inactivating the protein, at a rate k_F . Inactivated drug-protein targets dissociate
680 at a rate k_R . The first-order affinity of the drug to its protein target (K_D) is therefore the ratio of
681 the molecular dissociation rate to the molecular on-rate ($K_D = k_R/k_F$).

682 We stratify the entire bacterial population into $N+1$ subpopulations according to the
683 number i of inactivated drug-target complexes within each cell (i.e. the drug-target
684 occupancy), and we assume that growth and death rates of each bacterial cell depend on the
685 drug-target occupancy. That is, bacterial subpopulations with a larger drug-target occupancy
686 have slower growth rates and/or higher death rates than do bacterial subpopulations with a
687 smaller drug-target occupancy. Growth rate is therefore a monotonically decreasing discrete

688 function $G[i]$, and death rate is a monotonically increasing discrete function $D[i]$. We use
689 generalized logistic equations (**Supplementary Figure S1**) to describe overall growth and
690 death rates as a function of drug-target occupancy, allowing these functions to take the form
691 of a line, a sigmoidal curve, an exponential curve, or a step function. We assume that when a
692 drug inactivates all N protein targets in a cell, growth rate falls to zero (for bacteriostatic
693 drugs), death rate attains a maximal value D_N (for bactericidal drugs), or growth and death
694 rates are both affected (for drugs with mixed bactericidal and bacteriostatic action). In all of
695 these cases, the maximal rate of killing or growth attenuation can occur before all N target
696 proteins are inactivated if, for instance, $G[i]$ and/or $D[i]$ are step functions with inflection
697 points between 0 and N . During replication, a bacterial cell partitions its inactivated drug-
698 target complexes to two daughter cells according to a binomial distribution.

699 The change over time in the number of bacterial cells with exactly i inactivated drug-
700 target complexes (B_i) thus depends on the growth rate G_i , the death rate D_i , and the binding
701 kinetics of the drug to its protein target:

702 **[Equation 2]**

$$703 \quad \frac{dB_i(t)}{dt} = (i+1)k_R B_{i+1} + (N-(i-1))k_F C_0 B_{i-1} - ik_R B_i - (N-i)k_F C_0 B_i - D_i B_i - G_i B_i + \sum_{j=i}^N 2 \frac{\binom{j}{i}}{2^j} G_j B_j$$

704 The first four terms on the right side of this equation describe changes in B_i due to drug-target
705 binding and unbinding. The fifth term describes bacterial death, and the sixth and seventh
706 terms describe bacterial growth. We can then define $B(t)$ as a vector whose elements comprise
707 the set of all bacterial subpopulations ($B_0, B_1, \dots, B_i, \dots, B_{N-1}, B_N$) at a given time. Because
708 **Equation 2** is linear, we can describe the temporal dynamics of the entire bacterial population
709 with this vector, whose representation is a system of linear differential equations:

710 **[Equation 3]**

711
$$\frac{d\vec{B}(t)}{dt} = A\vec{B}$$

712 In the equation above, A denotes the matrix of coefficients describing the system of equations
713 for the vector $B(t)$. The values for the coefficients in A depend on the concentration C_o of drug,
714 on the drug's binding kinetics, and on the growth and death rate functions $G[i]$ and $D[i]$.

715 **Equation 3** represents an initial value problem. This system of linear differential
716 equations with a constant coefficient matrix has a unique solution given by

717 [Equation 4]

718
$$\vec{B}(t) = e^{At}\vec{B}_0$$

719 where the vector \vec{B}_0 denotes the initial composition of bacterial subpopulations at $t = 0$. The
720 solution can also be written as a linear superposition of a product of complex exponentials
721 (with arguments determined by eigenvalues) and polynomials (whose degree is determined by
722 the geometric multiplicity of these eigenvalues and whose coefficients are uniquely
723 determined by the initial conditions). In practice, $B(t)$ describes a family of exponential growth
724 and decay curves that represent the replication and death of all $N+1$ bacterial subpopulations
725 over time (**Figure 1B**). We solve for $B(t)$ numerically by calculating the matrix exponential of A
726 using a scaling and squaring algorithm implemented in MATLAB (MathWorks, Newton, MA)
727 (Al-Mohy & Higham, 2009).

728

729 *Calculation of minimum inhibitory concentration*

730 We define the MIC as the concentration C_o of an antibiotic such that any concentration of
731 drug at or above C_o is guaranteed to cause the eventual extinction of the bacterial population.

732 This occurs precisely when one eigenvalue of matrix A (from **Equation 3**) is zero and all other
733 eigenvalues have a negative real component. We thus express the MIC as

734 [Equation 5]

735
$$MIC = \inf\{C_0 > 0 \mid \max(\text{Re}(\text{eig}(A))) = 0\}.$$

736 With this formulation, finding the MIC amounts to finding the value of C_0 such that the
737 greatest real component of the eigenvalues of A is zero. Deriving the expression for the MIC in
738 the simplest case of the model, when $N = 1$, serves to illustrate this approach. For the purposes
739 of this derivation, we consider a drug that elicits both a bactericidal and a bacteriostatic effect,
740 so $G[i = 1] = 0$ and $D[i = 1] = D_N$. However, the approach for finding the MIC is identical for any
741 mechanism of drug action. The matrix A describing all bacterial subpopulations ($B_{i=0}$ and $B_{i=1}$)
742 in this simple case is

743 [Equation 6]

744
$$A = \begin{bmatrix} G_0 - k_F C_0 & k_R \\ k_F C_0 & -(k_R + D_N) \end{bmatrix}.$$

745 We wish to find the concentration C_{MIC} of antibiotic that yields negative real components of
746 all but one eigenvalues λ of matrix A . For the 2-by-2 matrix given by Equation 6, the
747 characteristic polynomial is given by $\lambda^2 - \text{tr}(A)\lambda + \det(A)$, and the Routh-Hurwitz stability
748 criterion needed to satisfy the negative value constraints on λ is $\text{tr}(A) \leq 0$ and $\det(A) \geq 0$. For the
749 matrix described in Equation 6, these expressions correspond to

750 [Equation 7]

751
$$G_0 - k_F C_0 - k_R - D_N \leq 0$$

752 and

753 [Equation 8]

754
$$(G_0 - k_F C_0)(-k_R - D_N) - k_F k_R C_0 \geq 0.$$

755 Solving for the concentration C_0 in both of these cases yields

756 [Equation 9]

757
$$C_0 \geq \frac{G_0 - k_R - D_N}{k_F}$$

758 in the case of Equation 7 and

759 [Equation 10]

760
$$C_0 \geq \frac{(k_R + D_N)G_0}{k_F D_N}$$

761 in the case of **Equation 8**. We expect the value of k_R to be greater than that of G_0 (that is, we
762 expect the rate of drug-target unbinding to be greater than the rate of bacterial replication).
763 We also expect the value of the death rate at saturating drug concentrations (D_N) to be
764 nonzero and positive. Therefore, **Equation 9** is guaranteed to be satisfied if **Equation 10** is also
765 satisfied. We thus find the expression for the MIC to be

766 [Equation 11]

767
$$C_{MIC} = \frac{(k_R + D_N)G_0}{k_F D_N}.$$

768 From this expression, we can infer the following proportionalities for the value of the MIC
769 relative to the values of other model parameters:

770 [Equation 12]

771
$$C_{MIC} \propto G_0$$

772
$$C_{MIC} \propto 1/k_F$$

773
$$C_{MIC} \propto k_R.$$

774 Polynomial expressions for the MIC, as shown in **Equation 11**, become exceedingly
775 complex beyond $N = 3$. However, we conjecture (although we have not been able to prove)
776 that the structure of the linear system shown in **Equation 3** guarantees the existence of the
777 MIC. For larger values of N , we leverage numerical schemes to calculate the eigenvalues of
778 matrix A . We use MATLAB's $eig()$ function, which calculates eigenvalues using the QZ
779 algorithm (Moler & Stewart, 1973).

780

781 *Model calibration via simulated annealing*

782 Numerical values for the model parameters N , D_o , μ_R , and μ_C were obtained from the literature
783 (Table 1). The values for G_o and D_N were obtained by fitting experimental kill curves at drug
784 concentrations of zero and 2.19 $\mu\text{g/ml}$, respectively, to exponential functions (Supplementary
785 Figure S11). We leveraged an adaptive simulated annealing algorithm coupled with local
786 gradient descent to obtain the remaining parameters (k_F , k_R , α_G , α_D , γ_G , and γ_D). Detailed
787 descriptions of the adaptive simulated annealing algorithm are available elsewhere
788 (Henderson, Jacobson, & Johnson, 2003; Ingber, 1995); in brief, simulated annealing is a global
789 optimization algorithm capable of escaping local minima. It is therefore well suited to
790 applications involving the optimization of many parameters. Adaptive simulated annealing is
791 a variant on the classical simulated annealing algorithm that probes global parameter space
792 with greater efficiency by accounting for each parameter's magnitude when formulating a
793 new parameter set at every iteration of the algorithm. We used adaptive simulated annealing
794 to minimize the difference between experimental time-kill curves and model simulations of
795 bacterial populations challenged to the same antibiotic doses. The difference between
796 experimental observation and simulation is expressed through the objective function, whose
797 value ψ the adaptive simulated annealing algorithm seeks to minimize:

798 [Equation 13]

$$799 \quad \psi = \sum_i \sum_j (W |E - B|)^2.$$

800 E denotes an m -by- n matrix of experimentally-measured population sizes at m drug
801 concentrations and n timepoints, B denotes simulated population sizes at the same drug
802 concentrations and timepoints, and W denotes an m -by- n weighting matrix (for our
803 application, simply a matrix of ones). B is a function of the parameters being optimized (that
804 is, $B = f(k_F, k_R, \alpha_G, \alpha_D, \gamma_G, \gamma_D)$).

805 Coupling the adaptive simulated annealing optimization with a local gradient descent
806 assures that our calibration procedure always converges on a local minimum. We used an
807 exponential cooling schedule for the simulated annealing algorithm, which assures that the
808 optimization runs ergodically (Ingber, 1995). That is, repeating the optimization many times
809 from random initial starting conditions in parallel yields roughly the same results as running
810 the optimization once for a very long time. This allowed us to parallelize the optimization
811 procedure by running the algorithm repeatedly across several cores of a computer and to
812 characterize the distributions of parameter values obtained from these calibrations
813 (**Supplementary Figure S3**). After performing 249 independent model calibrations, we
814 selected the parameter set with the lowest objective function value to use in subsequent
815 simulations. The parameter values for this set are shown in **Table 1**. Parameter sets for all
816 model optimizations performed are available in **Supporting Data File 3**.

817

818 *Simulating the emergence of secondary mutations*

819 We assumed that drug-resistant bacterial strains with secondary mutations that compensate
820 for fitness costs and/or that further increase MIC emerge from preexisting drug-resistant
821 subpopulations present in the initial population at the start of treatment (**Supplementary**
822 **Figure S8**). The size of the drug-resistant subpopulation at treatment onset ($B_{o,R}$) is given by
823 the mutation-selection balance, which expresses the size of the drug-resistant subpopulation
824 at which the rate of emergence of drug resistance alleles by spontaneous mutation equals the
825 rate of elimination of those alleles due to competitive fitness costs (Johnson, 1999):

826 [Equation 14]

$$827 \quad B_{o,R} = \frac{B_0 \mu_R}{c_R}$$

828 Here, μ_R denotes the mutation rate for drug resistance emergence per unit time.

829 In order to quantify the probability of secondary mutation emergence from this drug-
830 resistant subpopulation, we adapted a formulation that Lipsitch and Levin developed to study
831 the evolution of drug-resistant bacterial strains during antibiotic treatment (Lipsitch & Levin,
832 1997). We assumed that secondary mutations emerge exclusively due to errors in DNA
833 replication during bacterial growth. The expected number of resistant cells with secondary
834 mutations that emerge from a bacterial population with i inactivated drug-target complexes
835 ($E(M_{RC,i})$) is proportional to the total number of replications that the subpopulation undergoes
836 before extinction and the rate of secondary mutation emergence:

837 [Equation 15]

$$838 \quad E(M_{RC,i}) = \mu_C \int_0^{t_{EXT,i}} G_{R,i} B_{R,i}(t) dt$$

839 In this equation, μ_C denotes the secondary mutation rate, $G_{R,i}$ represents the growth rate of a
840 resistant strain with exactly i inactivated drug-target complexes, $B_{R,i}(t)$ describes the
841 population dynamics of the i th drug-resistant bacterial subpopulation, and $t_{EXT,i}$ describes the
842 amount of time elapsed from treatment onset until the bacterial subpopulation is eliminated
843 ($B_{i,R} = 1$ when $t = t_{EXT}$). The total number $E(M_{RC})$ of resistant mutants with secondary mutations
844 that we expect to observe over the course of treatment is thus the sum of Equation 15 over all
845 values of i , and the probability P_{RC} that a compensated resistant mutant will emerge over the
846 course of treatment follows from the Poisson assumption that secondary mutations arise
847 stochastically and independently of other mutations:

848 [Equation 16]

$$849 \quad P_{RC} = 1 - e^{-(\sum_{i=0}^N E(M_{RC,i}))}$$

850 The summation term in Equation 16 describes the total number of resistant strains with
851 secondary mutations expected to emerge before extinction. This equation thus quantifies the

852 Poisson probability that at least one resistant strain with a secondary mutation will emerge
853 over the course of treatment.

854

855 *Code and data*

856 We wrote all code in MATLAB. All of the code written for this study is available as a software
857 package in **Supplementary File 1**. Experimental data represented in **Figures 2A and 2B** and in
858 **Supplementary Figure S4** are available within **Supporting Data Files 1, 2, and 4**, and the
859 parameter values for all iterations of model optimization are available in **Supporting Data**
860 **File 3**.

861

862

863 **Acknowledgements**

864 We extend sincere thanks to Sören Abel, Benjamin Akhuetie-Oni, and Laura Quinto for
865 helpful feedback on the manuscript.

866

867 **Author Contributions**

868 Conceptualization: P.AzW.

869 Data curation: C.H.

870 Formal analysis: L.C., C.H., F.C., P.AzW.

871 Funding acquisition: P.AzW., T.C.

872 Investigation: C.H., F.C., A.P.

873 Methodology: L.C., P.AzW., C.H., A.P.

874 Project administration: P.AzW., T.C.

875 Resources: A.P., T.C., P.AzW.

876 Software: C.H.

877 Validation: C.H., L.C.

878 Visualization: C.H.

879 Writing – Original draft preparation: C.H.

880 Writing – Review & editing: C.H., P.AzW., F.C., L.C., T.C.

881

882 **Competing interests**

883 The authors declare no competing interests.

884

885 **References**

886 Ahn, S. H., Kim, D. H., Lee, A. R., Kim, B. K., Park, Y. K., Park, E.-S., . . . Kim, K.-H. (2015).

887 Substitution at rt269 in Hepatitis B Virus Polymerase Is a Compensatory Mutation

888 Associated with Multi-Drug Resistance. *PloS one*, *10*(8).

889 doi:10.1371/journal.pone.0136728

890 Al-Mohy, A. H., & Higham, N. J. (2009). A New Scaling and Squaring Algorithm for the Matrix

891 Exponential. *SIAM Journal on Matrix Analysis and Applications*, *31*(3), 970-989.

892 doi:10.1137/09074721X

893 Andersson, D. I., & Hughes, D. (2010). Antibiotic resistance and its cost: is it possible to reverse

894 resistance? *Nature Reviews Microbiology*, *8*(4), 260-271. doi:10.1038/nrmicro2319

895 Andrews, J. M. (2001). Determination of minimum inhibitory concentrations. *The Journal of*

896 *Antimicrobial Chemotherapy*, *48 Suppl 1*, 5-16. doi:10.1093/jac/48.suppl_1.5

897 Billal, D. S., Feng, J., Leprohon, P., Légaré, D., & Ouellette, M. (2011). Whole genome analysis

898 of linezolid resistance in *Streptococcus pneumoniae* reveals resistance and compensatory

899 mutations. *BMC genomics*, *12*, 512. doi:10.1186/1471-2164-12-512

900 Björkman, J., Nagaev, I., Berg, O. G., Hughes, D., & Andersson, D. I. (2000). Effects of

901 Environment on Compensatory Mutations to Ameliorate Costs of Antibiotic Resistance.

902 *Science*, *287*(5457), 1479-1482. doi:10.1126/science.287.5457.1479

903 Blair, J. M. A., Webber, M. A., Baylay, A. J., Ogbolu, D. O., & Piddock, L. J. V. (2015).

904 Molecular mechanisms of antibiotic resistance. *Nature Reviews Microbiology*, *13*(1), 42-

905 51. doi:10.1038/nrmicro3380

906 Brochet, M., Couvé, E., Zouine, M., Poyart, C., & Glaser, P. (2008). A Naturally Occurring

907 Gene Amplification Leading to Sulfonamide and Trimethoprim Resistance in

908 *Streptococcus agalactiae*. *Journal of Bacteriology*, *190*(2), 672-680.

909 doi:10.1128/JB.01357-07

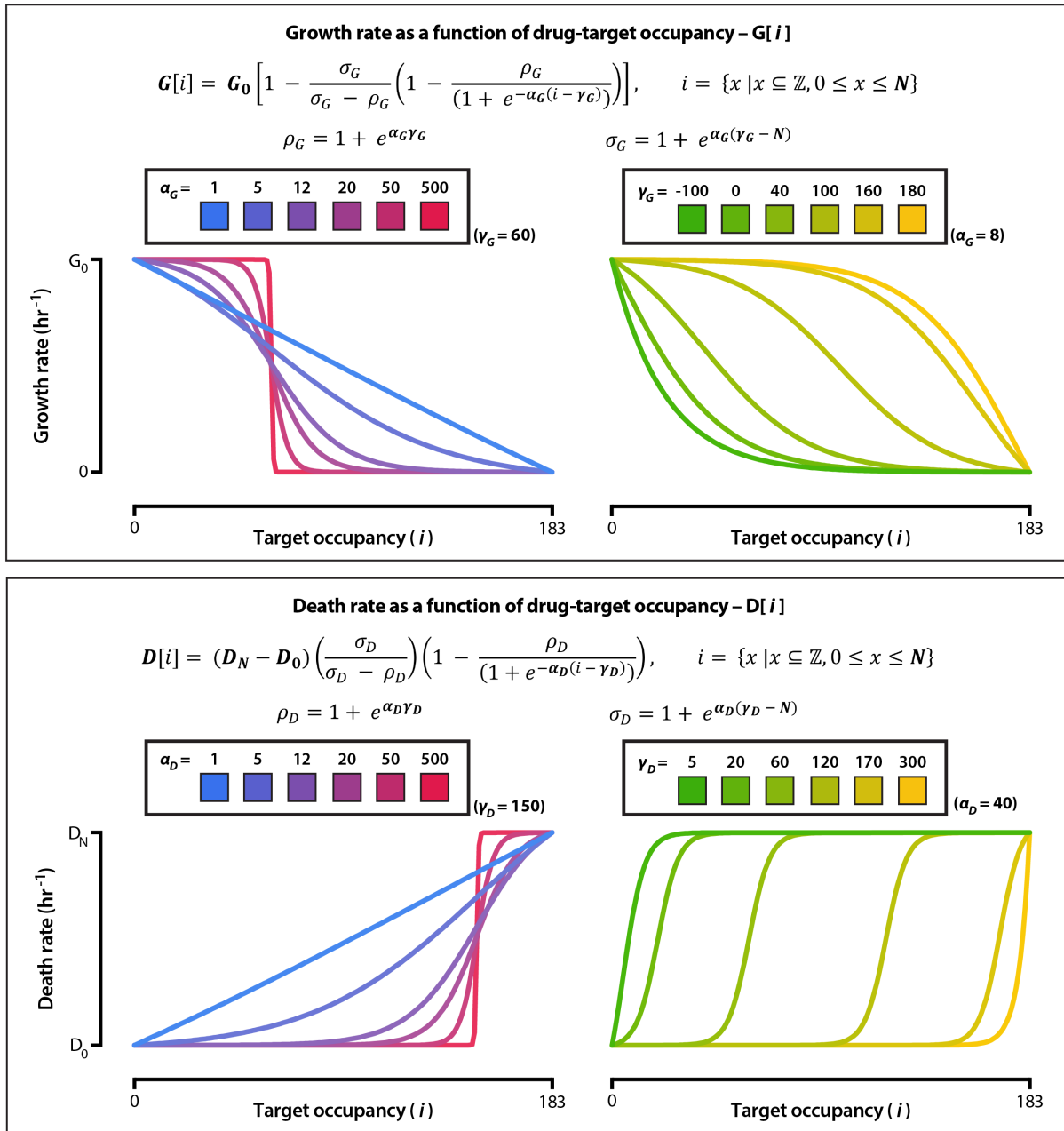
- 910 CDC. (2019). *Antibiotic Resistance Threats in the United States, 2019*. Retrieved from Atlanta,
911 GA:
- 912 Clarelli, F., Palmer, A., Singh, B., Storflor, M., Lauksund, S., Cohen, T., . . . Wiesch, P. A. z.
913 (2019). Drug-target binding quantitatively predicts optimal antibiotic dose levels.
914 *bioRxiv*, 369975. doi:10.1101/369975
- 915 Colijn, C., Cohen, T., Ganesh, A., & Murray, M. (2011). Spontaneous Emergence of Multiple
916 Drug Resistance in Tuberculosis before and during Therapy. *PloS one*, 6(3), e18327.
917 doi:10.1371/journal.pone.0018327
- 918 Cui, J., Liu, Y., Wang, R., Tong, W., Drlica, K., & Zhao, X. (2006). The mutant selection
919 window in rabbits infected with Staphylococcus aureus. *The Journal of Infectious*
920 *Diseases*, 194(11), 1601-1608. doi:10.1086/508752
- 921 Datsenko, K. A., & Wanner, B. L. (2000). One-step inactivation of chromosomal genes in
922 Escherichia coli K-12 using PCR products. *Proceedings of the National Academy of*
923 *Sciences of the United States of America*, 97(12), 6640-6645.
924 doi:10.1073/pnas.120163297
- 925 Day, T., Huijben, S., & Read, A. F. (2015). Is selection relevant in the evolutionary emergence
926 of drug resistance? *Trends in Microbiology*, 23(3), 126-133.
927 doi:10.1016/j.tim.2015.01.005
- 928 Dörr, T., Lewis, K., & Vulić, M. (2009). SOS Response Induces Persistence to Fluoroquinolones
929 in Escherichia coli. *PLOS Genetics*, 5(12), e1000760. doi:10.1371/journal.pgen.1000760
- 930 Drlica, K. (1999). Mechanism of fluoroquinolone action. *Current Opinion in Microbiology*, 2(5),
931 504-508.
- 932 Drlica, K., Malik, M., Kerns, R. J., & Zhao, X. (2008). Quinolone-mediated bacterial death.
933 *Antimicrobial Agents and Chemotherapy*, 52(2), 385-392. doi:10.1128/AAC.01617-06
- 934 Drlica, K., & Zhao, X. (2007). Mutant selection window hypothesis updated. *Clinical Infectious*
935 *Diseases: An Official Publication of the Infectious Diseases Society of America*, 44(5),
936 681-688. doi:10.1086/511642
- 937 Durão, P., Balbontín, R., & Gordo, I. (2018). Evolutionary Mechanisms Shaping the
938 Maintenance of Antibiotic Resistance. *Trends in Microbiology*, 26(8), 677-691.
939 doi:10.1016/j.tim.2018.01.005
- 940 Engelberg, H., & Artman, M. (1964). Studies on streptomycin-dependent bacteria: Effect of
941 streptomycin on protein synthesis by streptomycin-sensitive, streptomycin-resistant and
942 streptomycin-dependent, mutants of Escherichia coli. *Biochimica et Biophysica Acta*
943 *(BBA) - Specialized Section on Nucleic Acids and Related Subjects*, 80(2), 256-268.
944 doi:10.1016/0926-6550(64)90098-2
- 945 Everett, M. J., Jin, Y. F., Ricci, V., & Piddock, L. J. (1996). Contributions of individual
946 mechanisms to fluoroquinolone resistance in 36 Escherichia coli strains isolated from
947 humans and animals. *Antimicrobial Agents and Chemotherapy*, 40(10), 2380-2386.
- 948 Frenoy, A., & Bonhoeffer, S. (2018). Death and population dynamics affect mutation rate
949 estimates and evolvability under stress in bacteria. *PLOS Biology*, 16(5), e2005056.
950 doi:10.1371/journal.pbio.2005056
- 951 Gagneux, S., Long, C. D., Small, P. M., Van, T., Schoolnik, G. K., & Bohannan, B. J. M. (2006).
952 The Competitive Cost of Antibiotic Resistance in Mycobacterium tuberculosis. *Science*,
953 312(5782), 1944-1946. doi:10.1126/science.1124410
- 954 Gao, W., Chua, K., Davies, J. K., Newton, H. J., Seemann, T., Harrison, P. F., . . . Howden, B. P.
955 (2010). Two Novel Point Mutations in Clinical Staphylococcus aureus Reduce Linezolid

- 956 Susceptibility and Switch on the Stringent Response to Promote Persistent Infection.
957 *PLOS Pathogens*, 6(6), e1000944. doi:10.1371/journal.ppat.1000944
- 958 Gullberg, E., Cao, S., Berg, O. G., Ilbäck, C., Sandegren, L., Hughes, D., & Andersson, D. I.
959 (2011). Selection of Resistant Bacteria at Very Low Antibiotic Concentrations. *PLOS*
960 *Pathogens*, 7(7), e1002158. doi:10.1371/journal.ppat.1002158
- 961 Handel, A., Regoes, R. R., & Antia, R. (2006). The role of compensatory mutations in the
962 emergence of drug resistance. *PLoS computational biology*, 2(10), e137.
963 doi:10.1371/journal.pcbi.0020137
- 964 Harms, A., Maisonneuve, E., & Gerdes, K. (2016). Mechanisms of bacterial persistence during
965 stress and antibiotic exposure. *Science (New York, N.Y.)*, 354(6318).
966 doi:10.1126/science.aaf4268
- 967 Henderson, D., Jacobson, S. H., & Johnson, A. W. (2003). The Theory and Practice of Simulated
968 Annealing. In F. Glover & G. A. Kochenberger (Eds.), *Handbook of Metaheuristics* (pp.
969 287-319). Boston, MA: Springer US.
- 970 Hughes, D. (2014). Selection and evolution of resistance to antimicrobial drugs. *IUBMB life*,
971 66(8), 521-529. doi:10.1002/iub.1278
- 972 Ingber, L. (1995). *Adaptive Simulated Annealing: Lessons Learned*. Retrieved from McLean,
973 VA:
- 974 Isalan, M., Lemerle, C., Michalodimitrakis, K., Horn, C., Beltrao, P., Raineri, E., . . . Serrano, L.
975 (2008). Evolvability and hierarchy in rewired bacterial gene networks. *Nature*,
976 452(7189), 840-845. doi:10.1038/nature06847
- 977 Johnson, T. (1999). The approach to mutation-selection balance in an infinite asexual population,
978 and the evolution of mutation rates. *Proceedings. Biological Sciences*, 266(1436), 2389-
979 2397. doi:10.1098/rspb.1999.0936
- 980 Jungkind, D. L., & American Society for Microbiology Eastern Pennsylvania, B. (1995).
981 *Antimicrobial resistance: A crisis in healthcare*: Plenum Press.
- 982 Kampranis, S. C., & Maxwell, A. (1998). The DNA gyrase-quinolone complex. ATP hydrolysis
983 and the mechanism of DNA cleavage. *The Journal of Biological Chemistry*, 273(35),
984 22615-22626. doi:10.1074/jbc.273.35.22615
- 985 Kulesa, A., Kehe, J., Hurtado, J. E., Tawde, P., & Blainey, P. C. (2018). Combinatorial drug
986 discovery in nanoliter droplets. *Proceedings of the National Academy of Sciences*,
987 115(26), 6685-6690. doi:10.1073/pnas.1802233115
- 988 Leekha, S., Terrell, C. L., & Edson, R. S. (2011). General Principles of Antimicrobial Therapy.
989 *Mayo Clinic Proceedings*, 86(2), 156-167. doi:10.4065/mcp.2010.0639
- 990 Levin, B. R., Perrot, V., & Walker, N. (2000). Compensatory mutations, antibiotic resistance and
991 the population genetics of adaptive evolution in bacteria. *Genetics*, 154(3), 985-997.
- 992 Lindgren, P. K., Marcusson, L. L., Sandvang, D., Frimodt-Møller, N., & Hughes, D. (2005).
993 Biological Cost of Single and Multiple Norfloxacin Resistance Mutations in *Escherichia*
994 *coli* Implicated in Urinary Tract Infections. *Antimicrobial Agents and Chemotherapy*,
995 49(6), 2343-2351. doi:10.1128/AAC.49.6.2343-2351.2005
- 996 Lipsitch, M., & Levin, B. R. (1997). The population dynamics of antimicrobial chemotherapy.
997 *Antimicrobial Agents and Chemotherapy*, 41(2), 363-373.
- 998 Loftie-Eaton, W., Bashford, K., Quinn, H., Dong, K., Millstein, J., Hunter, S., . . . Top, E. M.
999 (2017). Compensatory mutations improve general permissiveness to antibiotic resistance
1000 plasmids. *Nature Ecology & Evolution*, 1(9), 1354. doi:10.1038/s41559-017-0243-2

- 1001 Lovmar, M., Nilsson, K., Lukk, E., Vimberg, V., Tenson, T., & Ehrenberg, M. (2009).
1002 Erythromycin resistance by L4/L22 mutations and resistance masking by drug efflux
1003 pump deficiency. *The EMBO Journal*, 28(6), 736-744. doi:10.1038/emboj.2009.17
- 1004 Maisnier-Patin, S., Berg, O. G., Liljas, L., & Andersson, D. I. (2002). Compensatory adaptation
1005 to the deleterious effect of antibiotic resistance in *Salmonella typhimurium*. *Molecular*
1006 *Microbiology*, 46(2), 355-366.
- 1007 Majcherczyk, P. A., Barblan, J.-L., Moreillon, P., & Entenza, J. M. (2008). Development of
1008 glycopeptide-intermediate resistance by *Staphylococcus aureus* leads to attenuated
1009 infectivity in a rat model of endocarditis. *Microbial Pathogenesis*, 45(5-6), 408-414.
1010 doi:10.1016/j.micpath.2008.09.003
- 1011 Martinez, J. L., & Baquero, F. (2000). Mutation frequencies and antibiotic resistance.
1012 *Antimicrobial Agents and Chemotherapy*, 44(7), 1771-1777. doi:10.1128/aac.44.7.1771-
1013 1777.2000
- 1014 Melnyk, A. H., Wong, A., & Kassen, R. (2015). The fitness costs of antibiotic resistance
1015 mutations. *Evolutionary Applications*, 8(3), 273-283. doi:10.1111/eva.12196
- 1016 Merker, M., Barbier, M., Cox, H., Rasigade, J.-P., Feuerriegel, S., Kohl, T. A., . . . Niemann, S.
1017 (2018). Compensatory evolution drives multidrug-resistant tuberculosis in Central Asia.
1018 *eLife*, 7, e38200. doi:10.7554/eLife.38200
- 1019 Mohamed, A. F., Cars, O., & Friberg, L. E. (2014). A pharmacokinetic/pharmacodynamic model
1020 developed for the effect of colistin on *Pseudomonas aeruginosa* in vitro with evaluation
1021 of population pharmacokinetic variability on simulated bacterial killing. *Journal of*
1022 *Antimicrobial Chemotherapy*, 69(5), 1350-1361. doi:10.1093/jac/dkt520
- 1023 Moler, C., & Stewart, G. (1973). An Algorithm for Generalized Matrix Eigenvalue Problems.
1024 *SIAM Journal on Numerical Analysis*, 10(2), 241-256. doi:10.1137/0710024
- 1025 Morgan-Linnell, S. K., & Zechiedrich, L. (2007). Contributions of the combined effects of
1026 topoisomerase mutations toward fluoroquinolone resistance in *Escherichia coli*.
1027 *Antimicrobial Agents and Chemotherapy*, 51(11), 4205-4208. doi:10.1128/AAC.00647-
1028 07
- 1029 Nemeth, J., Oesch, G., & Kuster, S. P. (2015). Bacteriostatic versus bactericidal antibiotics for
1030 patients with serious bacterial infections: systematic review and meta-analysis. *Journal of*
1031 *Antimicrobial Chemotherapy*, 70(2), 382-395. doi:10.1093/jac/dku379
- 1032 Nielsen, E. I., & Friberg, L. E. (2013). Pharmacokinetic-Pharmacodynamic Modeling of
1033 Antibacterial Drugs. *Pharmacological Reviews*, 65(3), 1053-1090.
1034 doi:10.1124/pr.111.005769
- 1035 Palmer, A. C., Chait, R., & Kishony, R. (2018). Nonoptimal Gene Expression Creates Latent
1036 Potential for Antibiotic Resistance. *Molecular Biology and Evolution*, 35(11), 2669-2684.
1037 doi:10.1093/molbev/msy163
- 1038 Palmer, A. C., & Kishony, R. (2013). Understanding, predicting and manipulating the genotypic
1039 evolution of antibiotic resistance. *Nature Reviews. Genetics*, 14(4), 243-248.
1040 doi:10.1038/nrg3351
- 1041 Palmer, A. C., & Kishony, R. (2014). Opposing effects of target overexpression reveal drug
1042 mechanisms. *Nature Communications*, 5, 4296. doi:10.1038/ncomms5296
- 1043 Pan, X. S., Yague, G., & Fisher, L. M. (2001). Quinolone resistance mutations in *Streptococcus*
1044 *pneumoniae* GyrA and ParC proteins: mechanistic insights into quinolone action from
1045 enzymatic analysis, intracellular levels, and phenotypes of wild-type and mutant proteins.

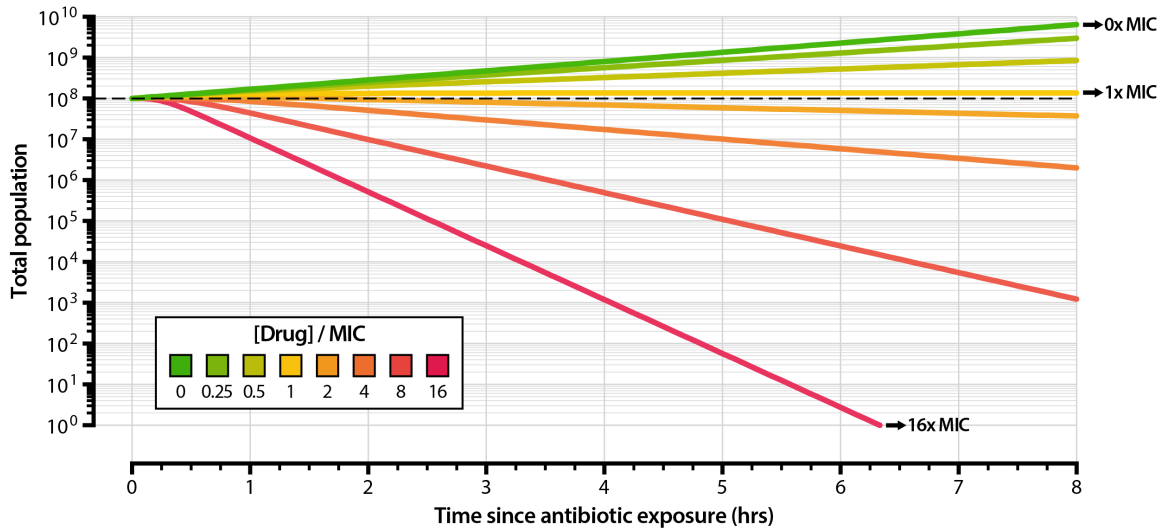
- 1046 *Antimicrobial Agents and Chemotherapy*, 45(11), 3140-3147.
1047 doi:10.1128/AAC.45.11.3140-3147.2001
- 1048 Pankey, G. A., & Sabath, L. D. (2004). Clinical Relevance of Bacteriostatic versus Bactericidal
1049 Mechanisms of Action in the Treatment of Gram-Positive Bacterial Infections. *Clinical*
1050 *Infectious Diseases*, 38(6), 864-870. doi:10.1086/381972
- 1051 Piddock, L. J. (1999). Mechanisms of fluoroquinolone resistance: an update 1994-1998. *Drugs*,
1052 58 Suppl 2, 11-18. doi:10.2165/00003495-199958002-00003
- 1053 Rao, G. G. (1998). Risk Factors for the Spread of Antibiotic-Resistant Bacteria. *Drugs*, 55(3),
1054 323-330. doi:10.2165/00003495-199855030-00001
- 1055 Redgrave, L. S., Sutton, S. B., Webber, M. A., & Piddock, L. J. V. (2014). Fluoroquinolone
1056 resistance: mechanisms, impact on bacteria, and role in evolutionary success. *Trends in*
1057 *Microbiology*, 22(8), 438-445. doi:10.1016/j.tim.2014.04.007
- 1058 Regoes, R. R., Wiuff, C., Zappala, R. M., Garner, K. N., Baquero, F., & Levin, B. R. (2004).
1059 Pharmacodynamic functions: a multiparameter approach to the design of antibiotic
1060 treatment regimens. *Antimicrobial Agents and Chemotherapy*, 48(10), 3670-3676.
1061 doi:10.1128/AAC.48.10.3670-3676.2004
- 1062 Roberts, J. A., Kruger, P., Paterson, D. L., & Lipman, J. (2008). Antibiotic resistance--what's
1063 dosing got to do with it? *Critical Care Medicine*, 36(8), 2433-2440.
1064 doi:10.1097/CCM.0b013e318180fe62
- 1065 Schoepp, N. G., Schlappi, T. S., Curtis, M. S., Butkovich, S. S., Miller, S., Humphries, R. M., &
1066 Ismagilov, R. F. (2017). Rapid pathogen-specific phenotypic antibiotic susceptibility
1067 testing using digital LAMP quantification in clinical samples. *Science Translational*
1068 *Medicine*, 9(410). doi:10.1126/scitranslmed.aal3693
- 1069 Schulz zur Wiesch, P., Engelstädter, J., & Bonhoeffer, S. (2010). Compensation of fitness costs
1070 and reversibility of antibiotic resistance mutations. *Antimicrobial Agents and*
1071 *Chemotherapy*, 54(5), 2085-2095. doi:10.1128/AAC.01460-09
- 1072 Shen, L. L., & Pernet, A. G. (1985). Mechanism of inhibition of DNA gyrase by analogues of
1073 nalidixic acid: The target of the drugs is DNA. *PNAS*, 82, 307-311.
- 1074 Silva, F., Lourenço, O., Queiroz, J. A., & Domingues, F. C. (2011). Bacteriostatic versus
1075 bactericidal activity of ciprofloxacin in *Escherichia coli* assessed by flow cytometry using
1076 a novel far-red dye. *The Journal of Antibiotics*, 64(4), 321-325. doi:10.1038/ja.2011.5
- 1077 Silver, L. L. (2011). Challenges of Antibacterial Discovery. *Clinical Microbiology Reviews*,
1078 24(1), 71-109. doi:10.1128/CMR.00030-10
- 1079 Siporin, C., Heifetz, C. L., & Domagala, J. M. (1990). *The new generation of quinolones*: M.
1080 Dekker.
- 1081 Stratton, C. W. (2003). Dead bugs don't mutate: susceptibility issues in the emergence of
1082 bacterial resistance. *Emerging Infectious Diseases*, 9(1), 10-16.
1083 doi:10.3201/eid0901.020172
- 1084 Thorpe, K. E., Joski, P., & Johnston, K. J. (2018). Antibiotic-Resistant Infection Treatment Costs
1085 Have Doubled Since 2002, Now Exceeding \$2 Billion Annually. *Health Affairs*, 37(4),
1086 662-669. doi:10.1377/hlthaff.2017.1153
- 1087 Vogwill, T., & MacLean, R. C. (2015). The genetic basis of the fitness costs of antimicrobial
1088 resistance: a meta-analysis approach. *Evolutionary Applications*, 8(3), 284-295.
1089 doi:10.1111/eva.12202

- 1090 Wang, P., Robert, L., Pelletier, J., Dang, W. L., Taddei, F., Wright, A., & Jun, S. (2010). Robust
1091 growth of *Escherichia coli*. *Current biology: CB*, *20*(12), 1099-1103.
1092 doi:10.1016/j.cub.2010.04.045
- 1093 WHO. (2012). *The evolving threat of antimicrobial resistance: options for action* (978-92-4-
1094 450318-8). Retrieved from <https://apps.who.int/iris/handle/10665/44812>
- 1095 WHO. (2014). *Antimicrobial resistance: Global report on surveillance*. Retrieved from Geneva:
- 1096 Wiesch, P. A. z., Abel, S., Gkatzis, S., Ocampo, P., Engelstädter, J., Hinkley, T., . . . Cohen, T.
1097 (2015). Classic reaction kinetics can explain complex patterns of antibiotic action.
1098 *Science Translational Medicine*, *7*(287), 287ra273-287ra273.
1099 doi:10.1126/scitranslmed.aaa8760
- 1100 Wiśniewski, J. R., & Rakus, D. (2014). Quantitative analysis of the *Escherichia coli* proteome.
1101 *Data in Brief*, *1*, 7-11. doi:10.1016/j.dib.2014.08.004
- 1102 Yu, G., Baeder, D. Y., Regoes, R. R., & Rolff, J. (2018). Predicting drug resistance evolution:
1103 insights from antimicrobial peptides and antibiotics. *Proceedings. Biological Sciences*,
1104 *285*(1874). doi:10.1098/rspb.2017.2687
- 1105 Zhang, Q., Sahin, O., McDermott, P. F., & Payot, S. (2006). Fitness of antimicrobial-resistant
1106 *Campylobacter* and *Salmonella*. *Microbes and Infection*, *8*(7), 1972-1978.
1107 doi:10.1016/j.micinf.2005.12.031
1108
1109



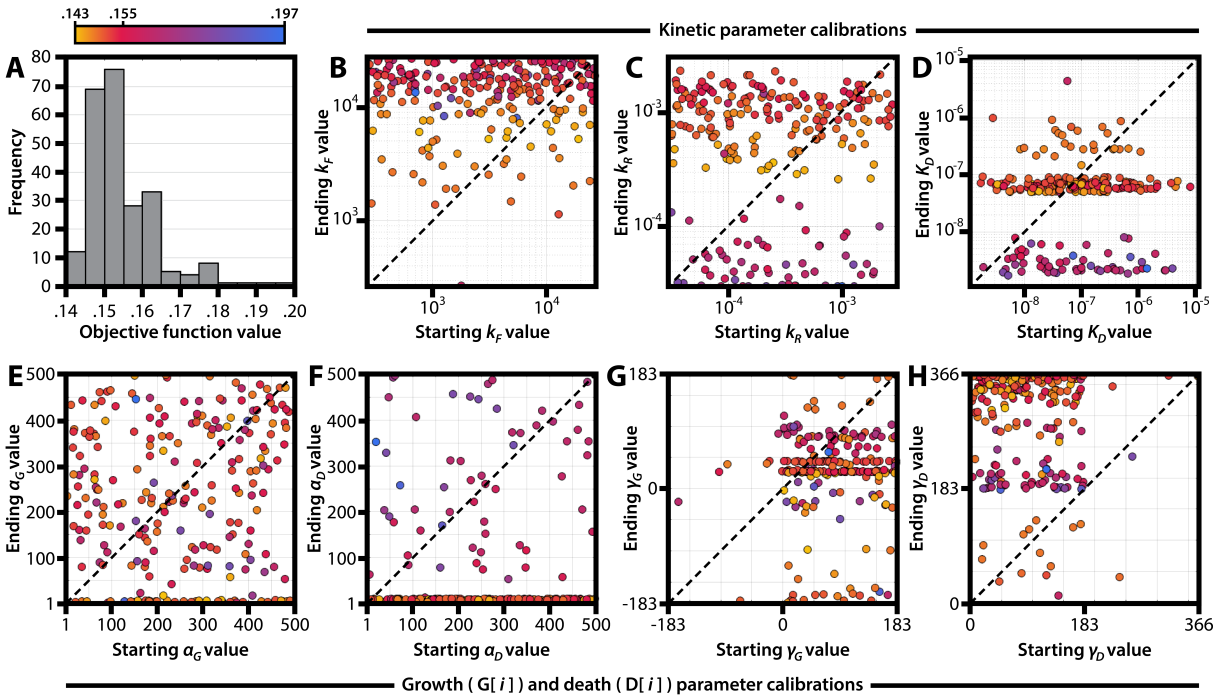
1110
1111
1112
1113
1114
1115
1116
1117
1118
1119
1120
1121
1122

Supplementary Figure S1 – Bacterial growth and death rates as a function of drug-target occupancy. We define the functions $G[i]$ and $D[i]$ as constrained logistic curves such that $G[i = 0] = G_0$, $G[i = N] = 0$, $D[i = 0] = D_0$, and $D[i = N] = D_N$. The parameters α_G and α_D define the steepness of the logistic curves for the growth and death rate function, respectively. α_G and α_D are unitless and range from 1 to 500; 1 yields a quasi-linear function, while 500 yields a quasi-step function. The parameters γ_G and γ_D define the inflection point of the logistic curves for the growth and death rate function, respectively. γ_G ranges from $-N$ to N and γ_D ranges from 0 to $2N$; the curve is quasi-sigmoidal if γ_G and γ_D are in between 0 and N and is quasi-exponential if γ_G and γ_D are outside of these bounds.



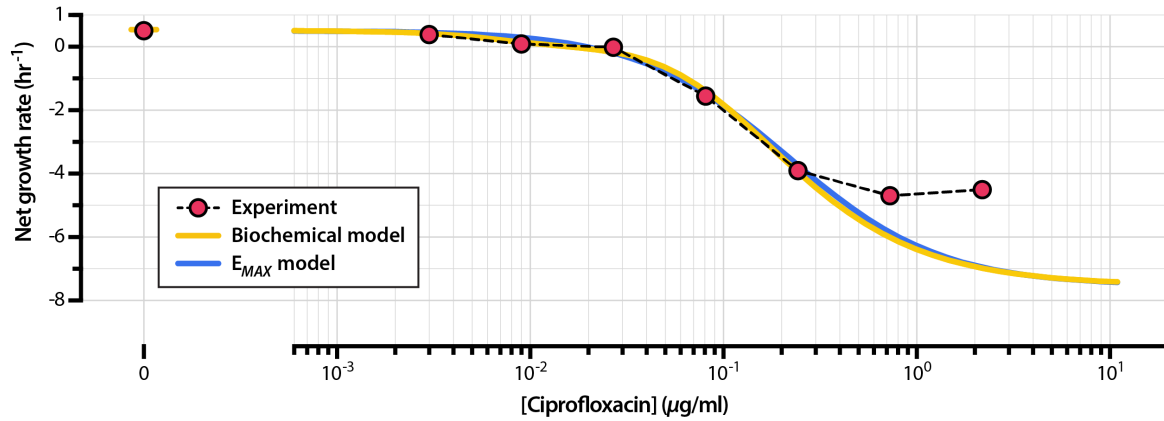
1123
1124
1125
1126
1127
1128
1129
1130
1131
1132

Supplementary Figure S2 – Simulated time-kill curves of *Escherichia coli* exposed to a range of drug concentrations. We used the parameter set outlined in Table 1 to model the growth and death of bacterial populations subjected to drug concentrations up to 16x minimum inhibitory concentration (MIC). Drug concentrations are expressed as factors of the MIC. The net growth rate of the entire bacterial population over the time course of the simulation decreases with increasing drug concentration.



1133
1134
1135
1136
1137
1138
1139
1140
1141
1142
1143
1144
1145
1146
1147
1148
1149
1150
1151

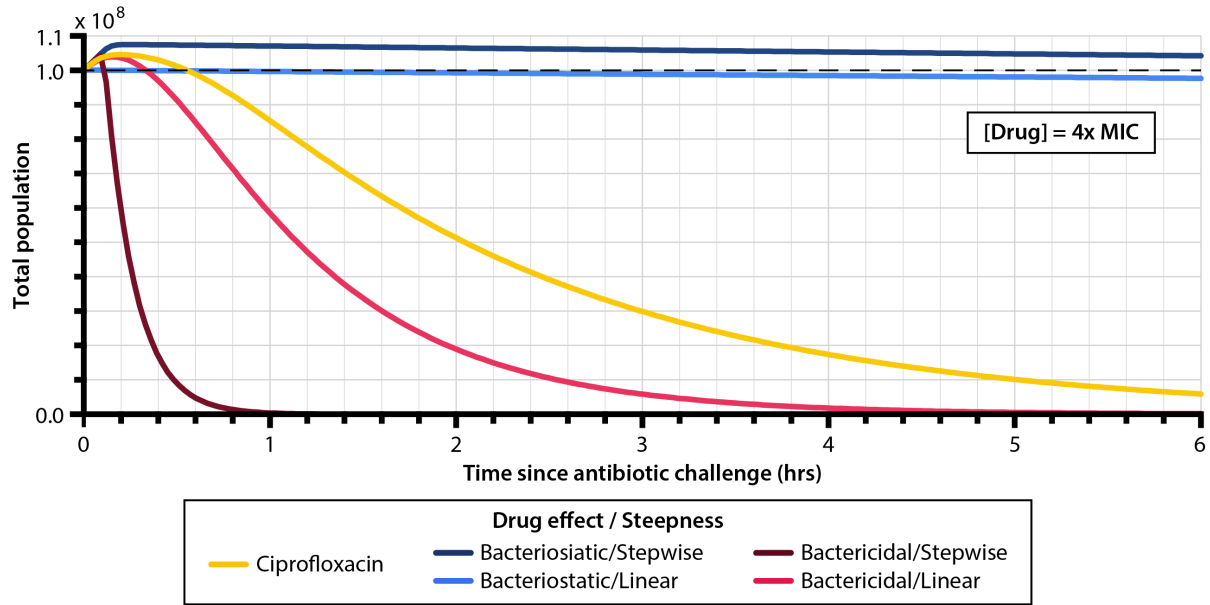
Supplementary Figure S3 – Results from 249 independent model calibrations to experimental data. We used adaptive simulated annealing coupled with gradient descent (see **Methods, Model calibration via simulated annealing**) to fit the model to experimental kill curve data of *E. coli* exposed to ciprofloxacin (**Supporting Data File 1**). Shown in this figure are the results for 249 independent model fits, each beginning with randomly-chosen values for the parameters describing drug-target binding rate k_F , drug-target unbinding rate k_R , steepness of the growth rate function α_G , steepness of the death rate function α_D , inflection point of the growth rate function γ_G , and inflection point of the death rate function γ_D . (A) Frequency distribution of objective function values obtained from independent model calibrations. The objective function value describes the goodness of the fit between experimental data and simulation; smaller values indicate higher goodness of fit. (B-H) Optimization plots showing randomly chosen initial parameter values (x-axis) and calibrated parameter values (y-axis) for all independent model calibrations. The optimized parameters are k_F (B), k_R (C), K_D (the ratio of k_R to k_F) (D), α_G (E), α_D (F), γ_G (G), and γ_D (H). The final objective function value of each model fit is colored according to the color bar above panel (A).



1152
1153

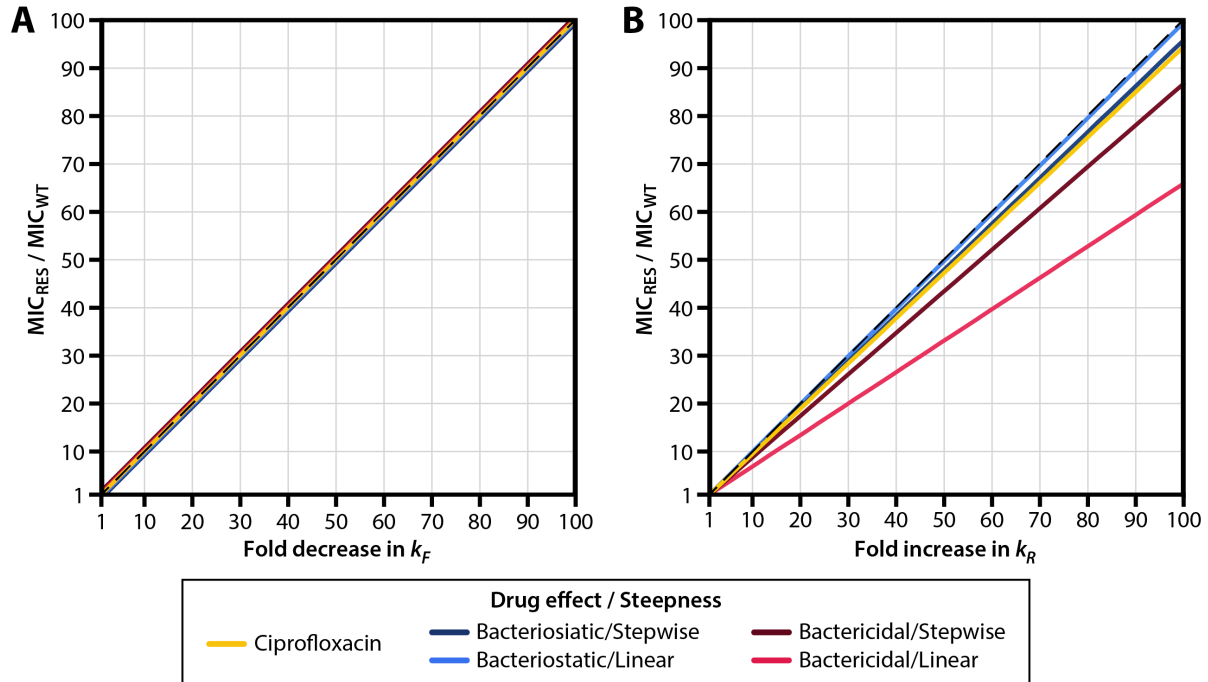
1154 **Supplementary Figure S4 – Pharmacodynamic curves generated from experimental data**
1155 **and from the calibrated model.** The experimental pharmacodynamic curve was generated
1156 by calculating the net growth rates of *E. coli* exposed to a set of ciprofloxacin drug
1157 concentrations (**Supporting Data File 1**). The time-kill curves of this same experimental
1158 dataset are shown in **Figure 2A**; see **Supporting Data File 4** for experimental data on net
1159 growth rate as a function of drug concentration. The model-calibrated pharmacodynamic
1160 curve was generated by simulating bacterial time-kill curves over the same range of drug
1161 concentrations used in the experiment and calculating associated net growth rates.

1162
1163



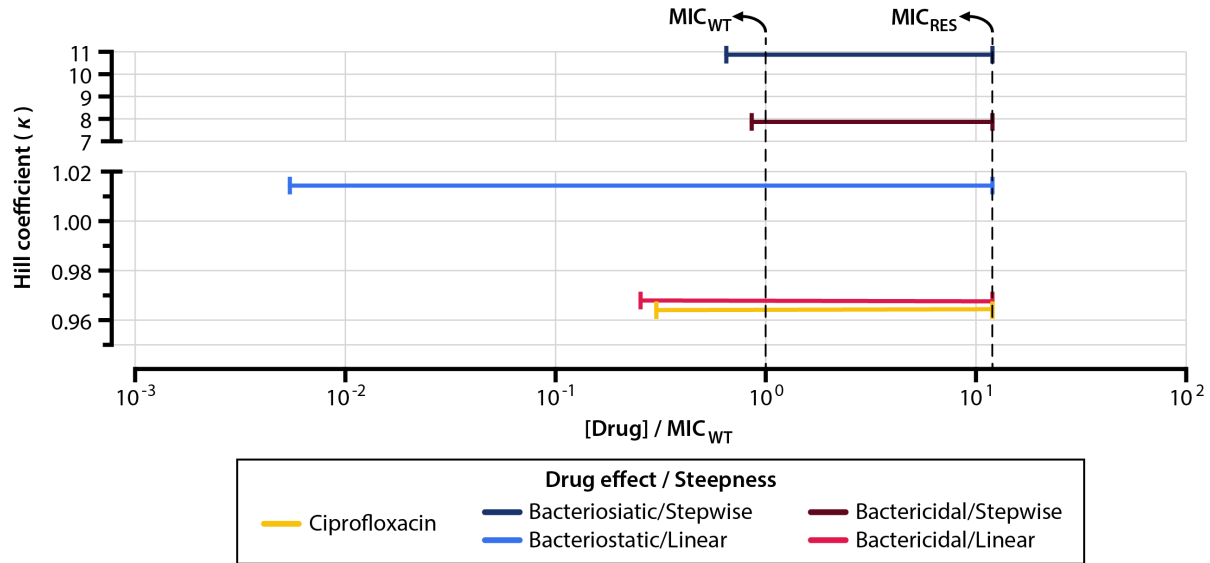
1164
1165
1166
1167
1168
1169
1170
1171
1172
1173

Supplementary Figure S5 – Simulated population curves for ciprofloxacin and for four extreme modes of antibiotic drug mechanism. We simulated a bacterial population of 10^8 cells exposed to antibiotic drug at $4x MIC$. The ciprofloxacin curve corresponds to the drug mechanism obtained from the model calibration to experimental data and detailed in **Figure 2C**, and the remaining curves correspond to the extreme schemes of drug mechanism shown in **Figure 2D**.



1174
1175
1176
1177
1178
1179
1180
1181
1182
1183
1184

Supplementary Figure S6 – MIC as a function of drug-target binding and unbinding kinetics. The MIC of a mutant (normalized to the MIC of the wild-type) is plotted against the fold-change in (A) drug-target binding (k_F) or (B) drug-target complex disassociation (k_R). For this simulation, mutants have no fitness costs associated with changes in k_F and k_R ($c_R = 0$). For drug-target binding (k_F), fold increase in MIC is directly proportional to fold decrease in k_F for all drug mechanisms. In both panels, the dashed line indicates the line of direct proportionality. MIC_{WT} : MIC of the wild-type strain; MIC_{RES} : MIC of the resistant strain.



1185
1186
1187
1188
1189
1190
1191
1192

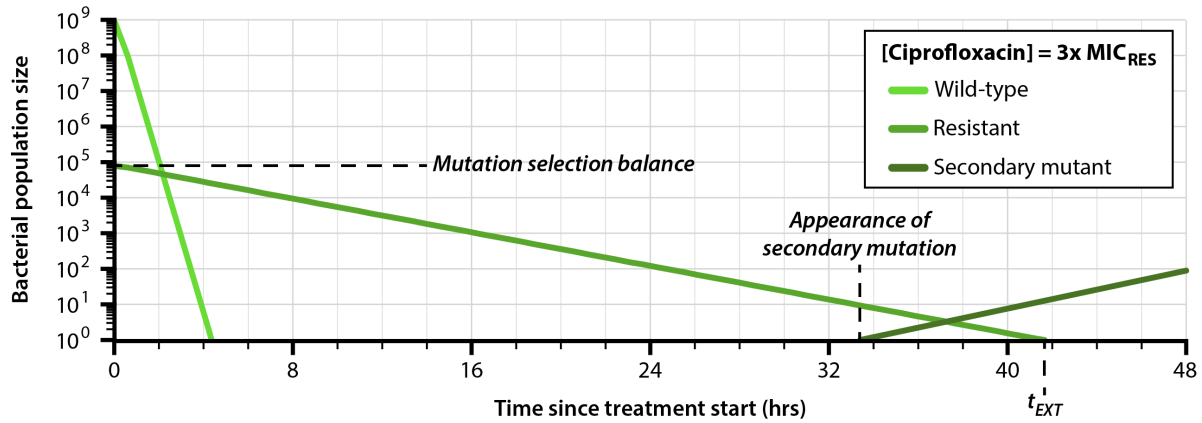
Supplementary Figure S7 – Drugs with steeper pharmacodynamic curves tend to have narrower resistance selection windows. To quantify the steepness of pharmacodynamic curves, we fit the curves for drug-resistant strains shown in **Figure 4C** to the pharmacodynamic function formulated by Regoes et al. (Regoes et al., 2004). The equation describes the net growth rate G_{net} of a bacterial population as a function of drug concentration C_o and other parameters (MIC , G_o , D_N) derived from the model:

1193

$$G_{net} = G_0 - \frac{(G_0 - D_N)(C_o/MIC)^\kappa}{(C_o/MIC)^\kappa - (D_N/G_0)}$$

1194
1195
1196
1197
1198
1199
1200
1201

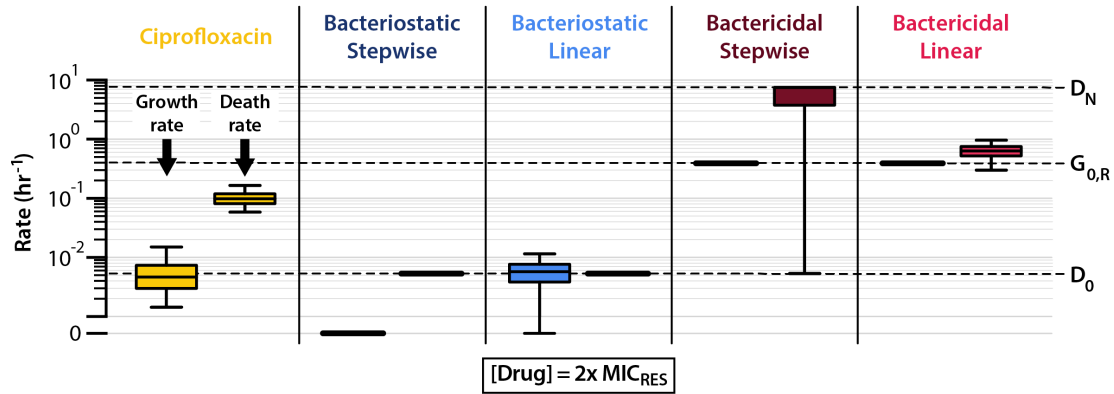
In this equation, κ describes the Hill coefficient, which serves as a measure of the steepness of the pharmacodynamic curve. Larger values of κ indicate steeper curves. For each of the drug mechanisms described in this study (**Supplementary Table 1**), we generated pharmacodynamic curves for drug-resistant mutants (**Figure 4C**, solid lines), determined the value of κ that best fits the curve, and plotted κ against the range of drug concentrations that represents the resistance selection window (**Figure 4D**). MIC_{WT} : MIC of the wild-type strain; MIC_{RES} : MIC of the resistant strain.



1202
1203

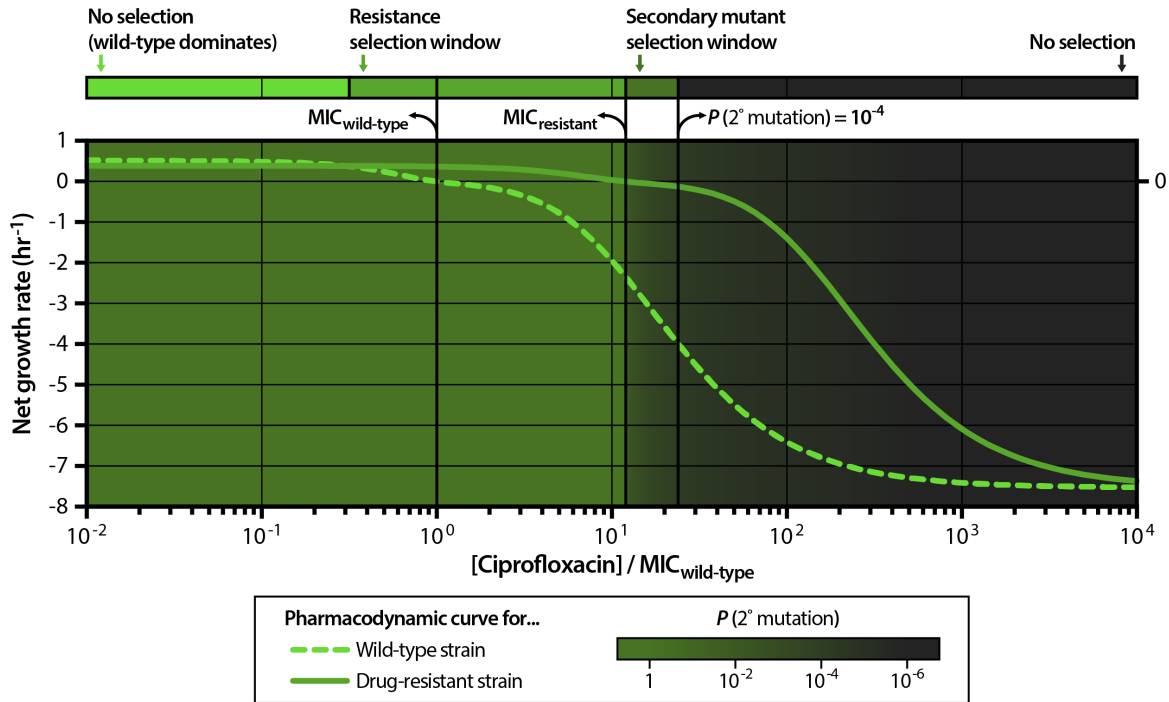
1204 **Supplementary Figure S8 – Emergence of secondary mutations within subpopulations of**
1205 **drug-resistant bacteria during antibiotic treatment.** When simulating the emergence of
1206 secondary mutations, we assume that a drug-resistant subpopulation (middle green) of
1207 bacteria is present at the start of treatment; the size of this subpopulation is given by the
1208 mutation selection balance of the allele that confers the drug-resistance phenotype (Johnson,
1209 1999). We calculate the probability that a drug-resistant strain with secondary mutations (dark
1210 green) emerges from this subpopulation before the elimination of the drug-resistant strain (at
1211 time t_{EXT}).

1212
1213



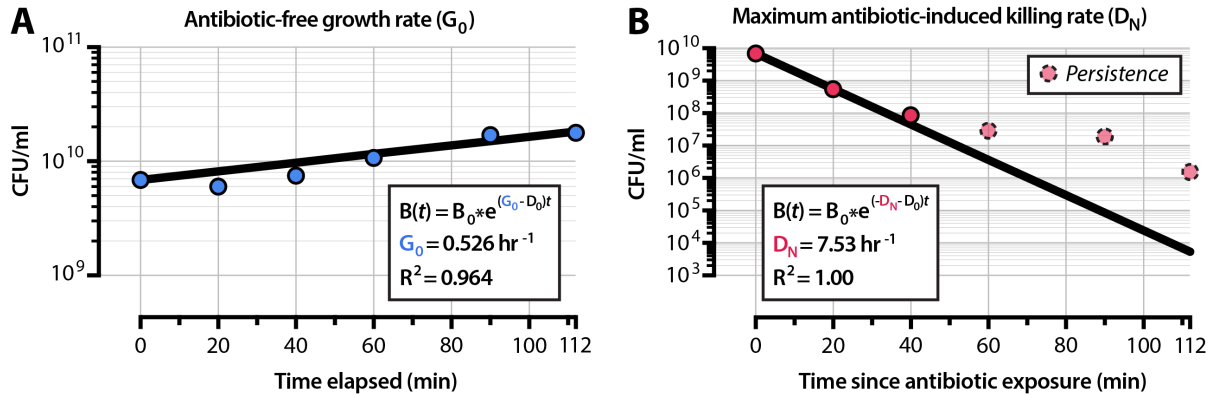
1214
1215
1216
1217
1218
1219
1220
1221

Supplementary Figure S9 – Distributions of growth and death rates for drug-resistant bacterial subpopulations undergoing steady-state exponential decline at 2x MIC_{RES}. Boxes denote the central 50% of the growth and death rate distributions, and whiskers denote the central 95% of the growth and death rate distributions.



1222
1223
1224
1225
1226
1227
1228
1229
1230
1231
1232
1233
1234
1235

Supplementary Figure S10 – The secondary mutant selection window. The secondary mutant selection window comprises the drug concentration range over which the net growth of the drug-resistant strain is negative but the probability of secondary resistance emergence before the end of treatment exceeds a defined threshold (in our simulations, 10^{-4} , or a 1 in 10,000 chance). Four regimes of selection exist: the null selection window in which the wild-type strain dominates, the resistance selection window, the secondary mutant selection window, and the complete killing window. We simplify these four regimes by disregarding the relative strengths of selection for each strain in each regime and we instead illustrate the boundaries of each region along a drug concentration axis (top bar); these simplified selection regimes are shown for all five drug mechanisms studied in Figure 5E.



1236
1237

1238 **Supplementary Figure SII – Obtaining G_o and D_N from experimental data.** (A) To obtain the
1239 value of G_o (growth rate in the absence of antibiotic) used in simulations, we fit an exponential
1240 growth curve to experimental data for *E. coli* cells grown in the absence of antibiotic. (B) To
1241 determine the value of D_N (maximum death rate in saturating conditions of antibiotic), we fit
1242 an exponential decay curve to experimental data for *E. coli* cells exposed to 2.19 $\mu\text{g/ml}$ of
1243 ciprofloxacin ($\sim 200 \times \text{MIC}$). The population size deviates from exponential decay at later
1244 timepoints (dashed and shaded) likely because of the emergence of persistent subpopulations
1245 of bacteria (Dörr et al., 2009). The R^2 values shown are the linear correlation coefficients for
1246 the model fit, and are not the correlation coefficients for the log-transform of the data.

1247
1248

1249

Drug mechanisms					
Activity	Ciprofloxacin	Bacteriostatic	Bacteriostatic	Bactericidal	Bactericidal
Steepness		Stepwise	Linear	Stepwise	Linear
Abbreviation	CIP	S/S	S/L	C/S	C/L
α_G	16.8	500	1	1	1
α_D	7.28	1	1	500	1
γ_G	24.8	35	35	35	35
γ_D	364	150	150	150	150
Bacteriostatic Potency	1	1	1	0	0
Bactericidal potency	1	0	0	1	1

1250

1251

1252

1253

1254

1255

1256

1257

1258

1259

1260

1261

1262

1263

1264

1265

Supplementary Table S1 – Parameters for a set of five drugs with different mechanisms of action. The parameters α_G and α_D describe the steepness of the growth and death rate functions, respectively, around the inflection point. The parameters γ_G and γ_D describe the inflection points of the growth and death rate functions (see **Supplementary Figure S1**). Bacteriostatic potency refers to the magnitude of growth rate decline at saturating concentrations of drug; a value of 1 indicates that that growth rate declines to zero in saturating concentrations of drug ($G[i = N] = 0$), and a value of 0 indicates that growth rate is unaffected by drug concentration ($G[i] = G_o$ for all i). Bactericidal potency refers to the magnitude of death rate increase at saturating conditions of drug; a value of 1 indicates that death rate increases to maximum in saturating concentrations of drug ($D[i = N] = D_N > D_o$), and a value of 0 indicates that death rate is unaffected by drug concentration ($D[i] = D_o$ for all i). All other parameters (including drug-target binding rate k_F , drug-target unbinding rate k_R , and target number N) are identical for all drugs in the set.

1266 **Supplementary File 1 – MATLAB code package containing the code written for this study.**
1267 This file contains scripts that we used to implement our model, to analyze data, and to
1268 generate the numeric values for all main text and supplementary figures.
1269
1270 **Supporting Data File 1 – Experimental data for the ciprofloxacin time-kill curve**
1271 **experiment represented in Figure 2A and Supplementary Figure S11.**
1272
1273 **Supporting Data File 2 – Experimentally-measured minimum inhibitory concentrations**
1274 **(MICs) for ciprofloxacin against *Escherichia coli* represented in Figure 2B.** We collated this
1275 list of experimentally-measured MICs from the literature; study sources are given in the file.
1276
1277 **Supporting Data File 3 – Model calibrations obtained via simulated annealing.** Starting and
1278 ending values for all model parameters are given for each iteration of the model fitting
1279 procedure described in **Methods, *Model calibration via simulated annealing.***
1280
1281 **Supporting Data File 4 – Experimental pharmacodynamic curve data represented in**
1282 **Supplementary Figure S4.** We generated these data by calculating the net growth rates of
1283 bacterial populations at each drug concentration listed in **Supporting Data File 1.**
1284